BRNO UNIVERSITY OF TECHNOLOGY

Vysoké učení technické v Brně

FACULTY OF ELECTRICAL ENGINEERING AND COMMUNICATION
DEPARTMENT OF ELECTRICAL POWER ENGINEERING

Fakulta elektrotechniky a komunikačních technologií
Ústav elektroenergetiky

Reconstruction of conductor movement and monitoring of high voltage lines
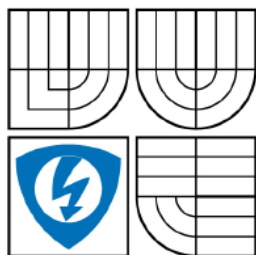
MASTER'S THESIS
Diplomová práce

AUTHOR   Bc. KAMIL ČERNÍN
Autor práce

BRNO 2009

VYSOKÉ UČENÍ
TECHNICKÉ V BRNĚ

Fakulta elektrotechniky
a komunikačních technologií

Ústav elektroenergetiky

Diplomová práce

magisterský navazující studijní obor
Elektroenergetika

Student: Bc. Kamil Černín   *ID:* 83085
Ročník: 2   *Akademický rok:* 2008/2009

NÁZEV TÉMATU:

Reconstruction of conductor movement and monitoring of high voltage lines

POKYNY PRO VYPRACOVÁNÍ:

1) Types of high voltage lines movements
2) Measuring devices
3) Reconstruction of movement based on measurement

DOPORUČENÁ LITERATURA:

Termín zadání: 9.2.2009   *Termín odevzdání:* 25.5.2009

Vedoucí práce: doc. Ing. Petr Toman, Ph.D.

doc. Ing. Petr Toman, Ph.D.
Předseda oborové rady

LICENČNÍ SMLOUVA
POSKYTOVANÁ K VÝKONU PRÁVA UŽÍT ŠKOLNÍ DÍLO

uzavřená mezi smluvními stranami:

1. Pan

Jméno a příjmení: Kamil Černín

Bytem: Dlouhá 54, Klobouky u Brna, 691 72

Narozen: 30.8.1985 v Hustopečích

(dále jen „autor")

a

2. Vysoké učení technické v Brně

Fakulta elektrotechniky a komunikačních technologií,

se sídlem Údolní 244/53, 602 00 Brno,

jejímž jménem jedná na základě písemného pověření děkanem fakulty:

doc. Ing. Petr Toman, Ph.D.

(dále jen „nabyvatel")

Čl. 1
Specifikace školního díla

1. Předmětem této smlouvy je vysokoškolská kvalifikační práce (VŠKP):
    - ☐ disertační práce
    - ☑ diplomová práce
    - ☐ bakalářská práce
    - ☐ jiná práce, jejíž druh je specifikován jako ....
    (dále jen VŠKP nebo dílo)

Název VŠKP:	Reconstruction of conductor movement and monitoring of high voltage lines
Vedoucí/ školitel VŠKP:	doc. Ing. Petr Toman, Ph.D.
Ústav:	Ústav elektroenergetiky
Datum obhajoby VŠKP:	

VŠKP odevzdal autor nabyvateli v[*]:

- ☑ tištěné formě   –   počet exemplářů 1ks
- ☑ elektronické formě   –   počet exemplářů 1ks

---

[*] hodící se zaškrtněte

2. Autor prohlašuje, že vytvořil samostatnou vlastní tvůrčí činností dílo shora popsané a specifikované. Autor dále prohlašuje, že při zpracovávání díla se sám nedostal do rozporu s autorským zákonem a předpisy souvisejícími a že je dílo dílem původním.
3. Dílo je chráněno jako dílo dle autorského zákona v platném znění.
4. Autor potvrzuje, že listinná a elektronická verze díla je identická.

Článek 2
Udělení licenčního oprávnění

1. Autor touto smlouvou poskytuje nabyvateli oprávnění (licenci) k výkonu práva uvedené dílo nevýdělečně užít, archivovat a zpřístupnit ke studijním, výukovým a výzkumným účelům včetně pořizovaní výpisů, opisů a rozmnoženin.
2. Licence je poskytována celosvětově, pro celou dobu trvání autorských a majetkových práv k dílu.
3. Autor souhlasí se zveřejněním díla v databázi přístupné v mezinárodní síti

   ▌ ihned po uzavření této smlouvy

   ☐ 1 rok po uzavření této smlouvy

   ☐ 3 roky po uzavření této smlouvy

   ☐ 5 let po uzavření této smlouvy

   ☐ 10 let po uzavření této smlouvy

   (z důvodu utajení v něm obsažených informací)
4. Nevýdělečné zveřejňování díla nabyvatelem v souladu s ustanovením § 47b zákona č. 111/ 1998 Sb., v platném znění, nevyžaduje licenci a nabyvatel je k němu povinen a oprávněn ze zákona.

Článek 3
Závěrečná ustanovení

1. Smlouva je sepsána ve třech vyhotoveních s platností originálu, přičemž po jednom vyhotovení obdrží autor a nabyvatel, další vyhotovení je vloženo do VŠKP.
2. Vztahy mezi smluvními stranami vzniklé a neupravené touto smlouvou se řídí autorským zákonem, občanským zákoníkem, vysokoškolským zákonem, zákonem o archivnictví, v platném znění a popř. dalšími právními předpisy.
3. Licenční smlouva byla uzavřena na základě svobodné a pravé vůle smluvních stran, s plným porozuměním jejímu textu i důsledkům, nikoliv v tísni a za nápadně nevýhodných podmínek.
4. Licenční smlouva nabývá platnosti a účinnosti dnem jejího podpisu oběma smluvními stranami.

V Brně dne: 11.5.2009

……………………………………..   ……………………………………

Nabyvatel   Autor

Bibliografická citace práce:

ČERNÍN, K., *Reconstruction of conductor movement and monitoring of high voltage lines.* Brno: Vysoké učení technické v Brně, Fakulta elektrotechniky a komunikačních technologií, 2009. 72 s. Vedoucí diplomové práce doc. Ing. Petr Toman, Ph.D.

Prohlašuji, že jsem svou diplomovou práci vypracoval samostatně a použil jsem pouze podklady (literaturu, projekty, SW atd.) uvedené v přiloženém seznamu.

…………………………

BRNO UNIVERSITY OF TECHNOLOGY

Faculty of Electrical Engineering and Communication

Department of Electrical Power Engineering

Master's Thesis

Reconstruction of conductor movement and monitoring of high voltage lines

by

Bc. Kamil Černín

Supervisor: doc. Ing. Petr Toman, Ph.D.

Brno University of Technology, 2009

Brno

ABSTRACT

This thesis deals with overhead power lines movement monitoring. This may cover voltages from 70 kV to 400 kV. Sensors are placed on the conductors and the main objective is to evaluate their mechanical behaviour from low frequencies (fraction of Hz) to high frequencies (some tens of Hz). This document has evaluated the possibilities to reproduce large low frequency movements as those observed in large turbulent wind, short-circuit, ice shedding, galloping or any other cause. This aims to help operators and designers make decisions. The robustness of the development includes the introduction/combination of new sensors, the appropriate mathematical development needed to reproduce what has been measured and this has been done on records obtained either by simulations, laboratory tests or actual measurements on line.

KEY WORDS: overhead power lines, vibrations, large movements, Kalman filter

ABSTRAKT

Tahle práce se zabývá monitorováním venkovních vysokonapěťových vedeních, což mohou být vedení od 70kV do 400kV. Senzory jsou umístěny na vodiči a hlavní myšlenkou je vyhodnotit mechanické chování vodičů, a to od nízkých frekvencí (zlomky Hz) až po vysoké frekvence (desítky Hz). Tahle práce se zabývala pohyby o nízkých frekvencích a vysokých amplitudách a popsala možnosti sestavení těchto pohybů na základě měření ze senzorů. Konkrétně se jedná o pohyby v případě silného větru, zkratu, opadávání ledu nebo dalších. Všechno tohle pomáhá operátorů dělat rozhodnutí ohledně provozování sítí. Vývoj zahrnuje přidání/kombinaci nových senzorů, popsání matematického algoritmu potřebného k sestavení pohybu na základě toho co bylo změřeno, ať už se jedná o hodnoty získané simulací, laboratorním testem nebo reálným měřením na vedení.

KLÍČOVÁ SLOVA: venkovní vysokonapěťová vedení, vibrace, nestandardní pohyby, Kalmanův filtr

CONTENTS

PICTURE CONTENTS

TABLE CONTENTS

TABLE OF SYMBOLS AND SHORTCUTS

Symbol	Quantity	Unit
a	acceleration	$m*s^{-2}$
$\mathbf{B}_k$	control-input model	
B,C,D	parametres of filter tuning	
dt	time increment	s
f	frequency	Hz
$\mathbf{F}_k$	state transition model	
$\mathbf{g}$	acceleration due to gravity	$m*s^{-2}$
$\mathbf{H}_k$	observation model	
I	identity matrix	
$\mathbf{K}_k$	*optimal* Kalman gain	
$\mathbf{P}_k$	error covariance matrix	
$\mathbf{Q}_k$	process noise covariance	
r	position	m
$\mathbf{R}_k$	measurement noise covariance	
$\mathbf{S}_k$	residual covariance	
t	time	s
$\mathbf{u}_k$	control vector	
v	velocity	$m*s^{-1}$
$\mathbf{v}_k$	measurement noise	
$\mathbf{w}_k$	process noise	
$\mathbf{x}_k$	state vector	
$\tilde{\mathbf{y}}_k$	measurement residual	
$\mathbf{z}_k$	measurement	
γ	angle between axe "x_r" and acceleration	° (rad)
φ	angle between axis	° (rad)
ω	angular velocity	$°*s^{-1}$ ($rad*s^{-1}$)

Subscripts:

0	initial condition	
k	step	
x,y,z	axis information	

Superscripts:

∧	estimate	
T	transpose of a matrix	

1 INTRODUCTION

Thermal rating of the lines depends on many parameters and factors like weather and current flow. And it is well known that thermal rating of lines changes continually, because parameters and factors included are changing continually as well. Transmission lines are designed in worst weather conditions (maximum solar heating, maximum external temperature, minimum wind speed ...) to control the maximum sag. But the experience shows that in practice, actual ambient conditions are less restrictive (generally more than 98% of the time) than those designed in the standards. So if we could have a possibility to measure the actual sag of lines in real time, we can better use existing overhead lines and save money for building new overhead lines. An increased ampacity of the conductor depending on the actual weather condition is thus generally available most of the time. Moreover there is still 2% of the time when actual weather conditions could be worse than those supposed and there exists risks. With real time sag monitoring device we know "exact" information about sag. All in all, real time monitoring is a quick applicable solution at a reasonable cost for better usage of existing overhead lines.
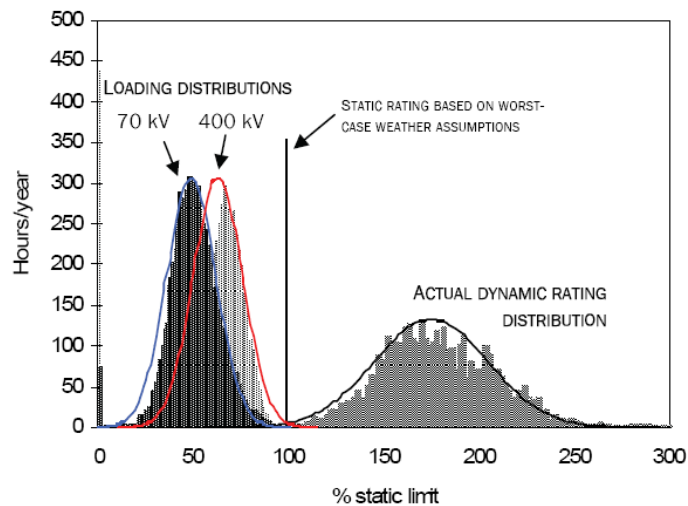
Figure 1-1 Comparison of Loading and actual Rating distributions [1]

In Figure 1-1 is a comparison of loading and actual rating distributions for an overhead line over one year. It shows virtual example based on actual loading for a 70 kV and 400 kV of Belgian line and actual rating based on a published case (Dale Douglas, PTI).

2 AMPACIMON®

Ampacimon device, system and method have been patented in September 2005, with a particular emphasis on EMC (electromagnetic compatibility) protection. Patent number: WO 2007/031435 (A1).

2.1 What is Ampacimon®

Due to increasing consumption of electrical energy, ampacity determination is a key factor for the huge market around the world. Especially operators of overhead high voltage lines are interested in upgrading existing overhead lines than building new ones. Still more important is the impact of market release in Europe and USA which will force to have real time information on main lines. In a deregulated market environment, the priority of the market is to maximize their profit. It means to maximize the ability of transmission in a secured way and to minimize serious disturbances and time of inactive lines. Moreover power systems in European regions as well as North American ones will be operated closer to their limits, because of difficulties to build new lines and growing demand of electric power in most countries. Under the above described stressed conditions, thermal overloads (causing sag) are critical threats to system operation. But there will be a greater possibility of cascade tripping. The Italian blackout (Sept 28th, 2003) as well as the New York blackout (August 14th, 2003) have their origin in a flashover between trees and power lines. More recently on November 4th, 2006 a major blackout in the whole Europe has been hopefully avoided. However; it affected 15 million people after the cascading event.

Figure 2-1 Black out in New York in 2003 [1]

2.2 Ampacimon® method

Ampacimon device allows real time monitoring of sag and other motion characteristics based on frequency analysis. Precision on sag is about 2%. Thanks to this low frequency analysis provided by accelerometers, Ampacimon device does not need any line nor any environmental data to determine the sag. Therefore, this method is more reliable than other determination methods.

Ampacimon device monitor even vibration (0 to 100Hz) to evaluate effects of fatigue. It helps to take preventive control of conductors and dampers.

Another advantage is that Ampacimon is autonomous (as it is directly powered by the line) and can be located anywhere on the span, it requires no calibration for first use, and moreover, it can be installed live-line in roughly 15 minutes. It saves lots of time and money.

Figure 2-2 Typical installation on live line in France at 90kV on HT ACSS conductor [1]

Figure 2-3 Live-line installation [1]
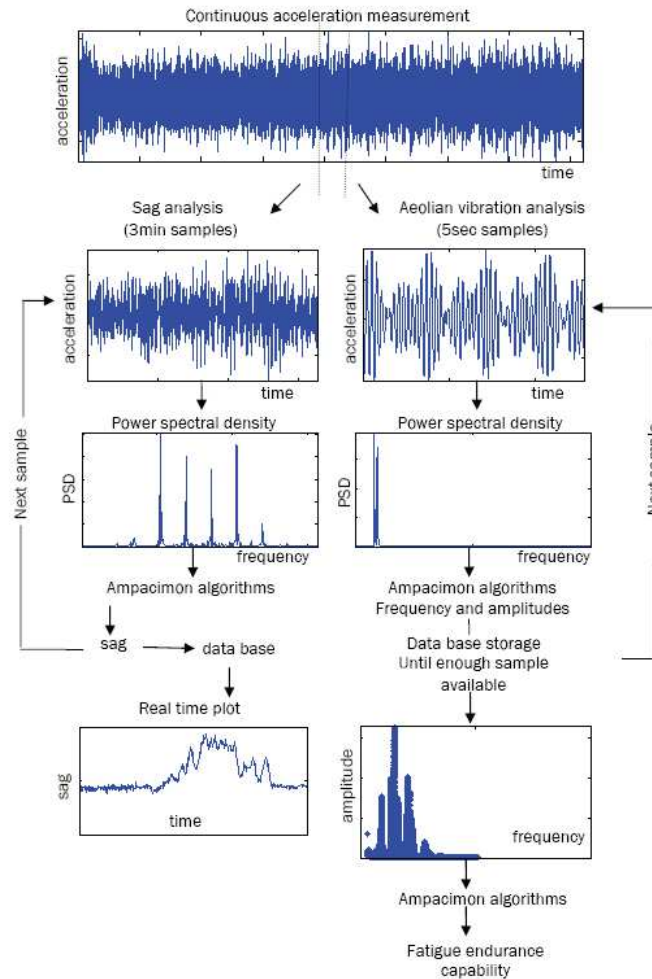
Figure 2-4 Ampacimon vibration analysis method to deduce line sag and material fatigue [1]
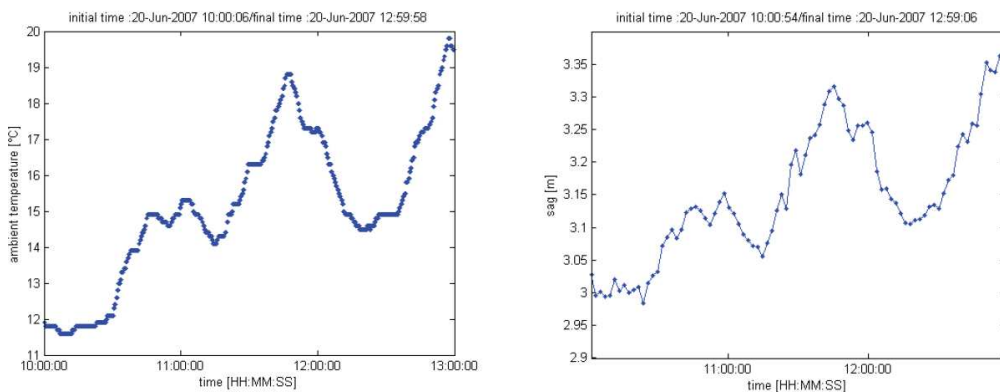
Figure 2-5 Ambient temperature and sag as deduced by Ampacimon vs. time [1]

2.3 Who is concerned by Ampacimon®?

Using real time systems increases thermal rating of lines of about 10 to 15 % on average. It could be higher in some cases depending on the previous design of the line. Information sent by Ampacimon are useful for the utilities using the lines as their business, to make a more efficient use of existing overhead lines and thus a better ROI, to be informed in real time of troubles on the network, to detect the lines on which vibrations levels are not sufficiently protected, to be informed about damages, to prevent black-outs limiting unnecessary cascade tripping, to evaluate the evolution of the fatigue of their lines, and to be informed early enough of incoming troubles

to inform their maintenance staff and/or to redirect the power flow not to loose customers, in other words, to save money. For the new developed overhead lines to better monitor their behaviour. (Real time sag, snow or ice overloads, reaction against wind blow, vibration level, etc.) All these advantages will help to maintain the customers in acceptable service conditions.
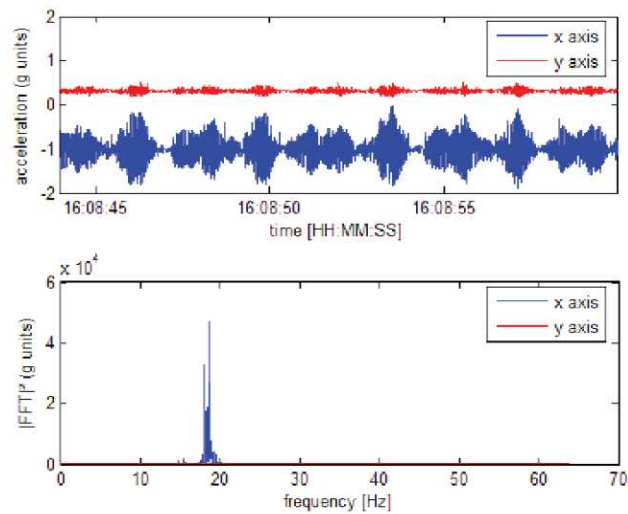
Figure 2-6 Typical Ampacimon outputs for Aeolian vibration analysis [1]

2.4 Design of Ampacimon®

The size of the last version of the device is 20x15 cm and it weighs about 7kg. Internal part is containing microelectronics and current transformer specially designed for Ampacimon application from 70 to 765kV. Anticorona designed. A special design is used to protect the wiring from short circuit currents, lightning over voltages. The power level demand of this system is a few Watts. The microelectronics system is equipped with four 2D accelerometers (in such a way that 3D movement can be analyzed). Measurement coming from gyroscopes could be added to the actual design. The sampling rate is about 200 Hz. Measurements are possible to send to the antennas. First antenna is a 433 MHz antenna with limited power emission (depending on local standards), able to transmit license free at about 100 m. Second one uses mobile phone network using frequencies 900/1800/1900 MHz. All materials are carefully chosen to be able to work with temperature ranging from -40°C to 85°C.

Figure 2-7 Typical installation on 220 kV line in Belgium (2005) [1]
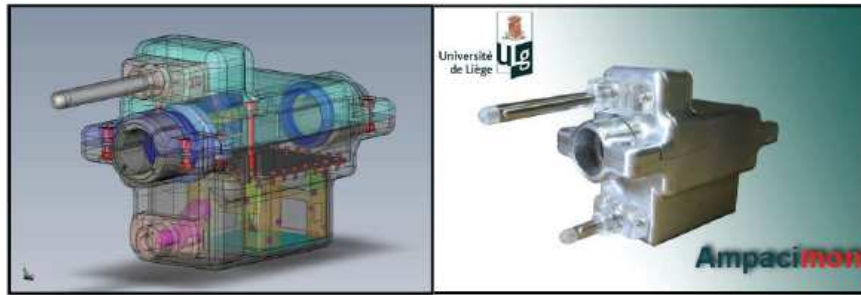
Figure 2-8 CAO view and actual view of the last version of Ampacimon (2008) [1]

3 CONDUCTOR MOTION

There are three main types of power line vibration (after Orawski 1993), indicating Aeolian vibration. This is shown in wake-induced oscillation and galloping, with their ranges of loop lengths and amplitude.
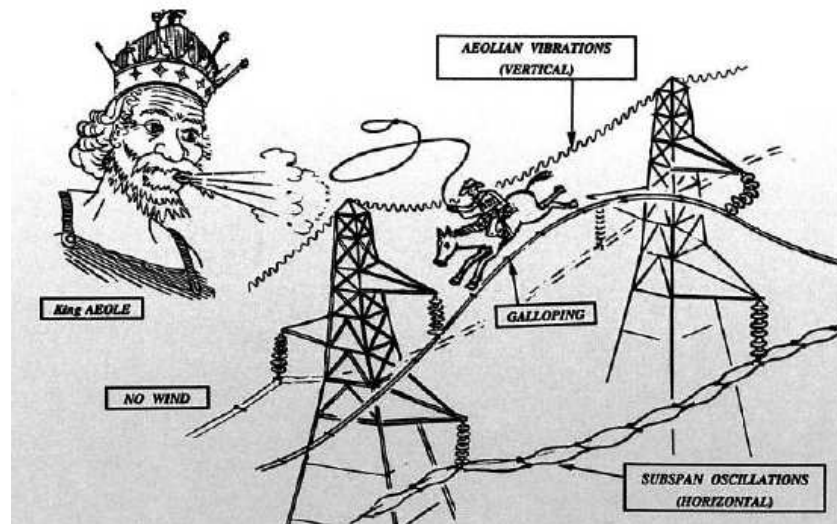
Figure 3-1 Three main types of conductor motion [2]

3.1 Aeolian vibrations

Aeolian vibration is one of the most prevalent problems in transmission lines. It causes fatigue failure of conductor strands or of other items associated with conductor. In low to moderate winds, this type of conductor motion can occur at almost any time and any transmission line. Reliable transmission-line design requires that Aeolian vibration of the conductors be controlled below critical levels to avoid fatigue damage.

Facts of Aeolian vibrations:

- Characteristic frequencies are in the approximate range of 3-200 Hz. The frequency range depends on many conditions. Mainly the size and tensile load of the conductor. Lower frequencies are typical for large conductors in low winds, while upper frequencies are typical for small ground wires in moderate winds.

- Maximum possible amplitude is equal to the conductor diameter.

- Records of vibration at a point on a conductor show Figure 3-2

- Conductor vibration causes localized bending, which depends on its level, causes fatigue failures of the conductor strands or the clamps of spacers and other devices installed on the conductor. The conductor vibration may also cause fatigue damage to items associated with the support and protection of the conductor itself – tower arms, spacers and dampers.

- The most serious Aeolian vibrations occurs when the conductor tensions are high, the terrain is smooth, with frequent, low-to-moderate, steady winds, and the spans are long.

- There is a possibility to control this vibration using dampers.
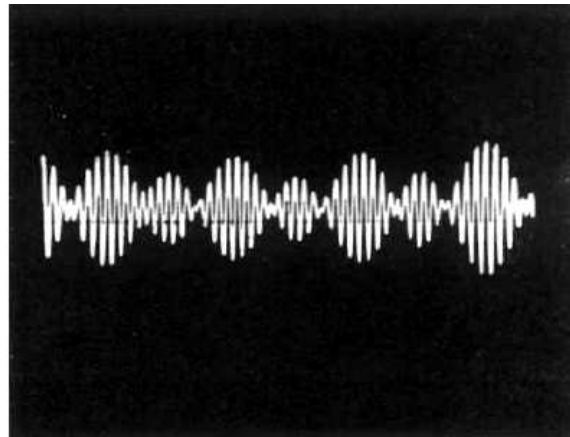
Figure 3-2 Record of vibration at a point on a conductor. [2]

Figure 3-3 Fatigue failure of conductor strands at the suspension clamp. [2]

The design of transmission line is made to control Aeolian vibrations of conductors below critical levels to avoid fatigue damage. With the design rules based on past experiences we are able to know strength of the Aeolian vibrations. We can also measure existing lines to know the conditions using special-purpose measuring instruments.

The second way to identify the conditions is by using the analytical approach to stimulate behaviour of the conductor and other related devices. This approach can be used successfully to investigate alternatives in design process, also in the direct design of the damping system for a new line. The most used analytical models are based on the Energy Balance Principle (EBP), and they give an estimate of expected vibratory motions. These kinds of things are described in [1], I didn't use the analytical models.

When it was recognized that conductor strand failure causes Aeolian vibration, a number of protection devices were developed following two main concepts. The first concept sought to provide reinforcement against the effect of vibration of the conductor. The second concept took into consideration the application of energy-dissipating devices, which were able to reduce the level of conductor Aeolian vibrations. The second method was soon recognized as the most practical and effective method, and a number of vibration dampers have been developed to date.
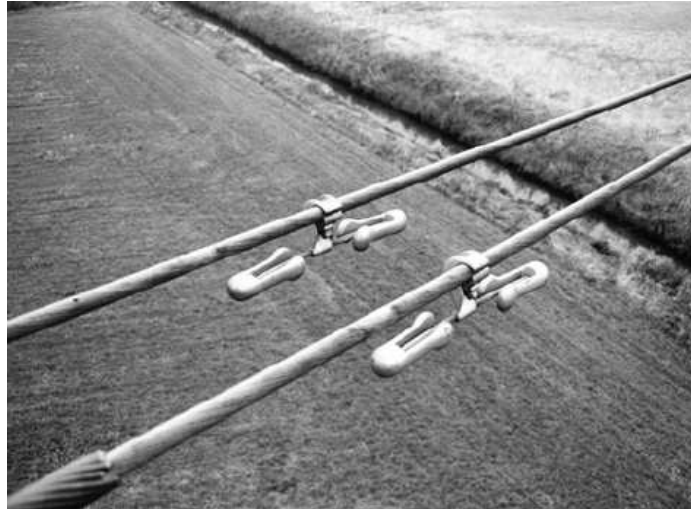
Figure 3-4 Vibration dampers [2]
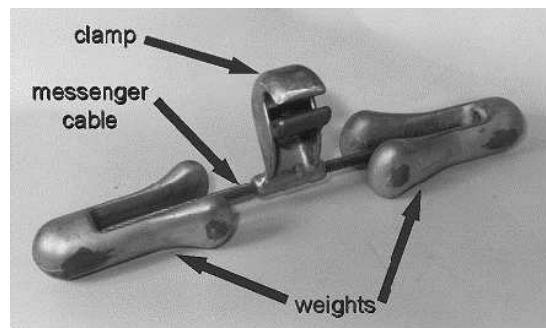
Figure 3-5 Vibration damper of Stockbridge type [2]

3.2 Fatigue

The most common form of damage resulting from Aeolian vibration is fatigue failure of strands in overhead conductors. But influenced are other line components such as armour rods, dampers, ties, insulators, and tower members. Conductor fatigue may also result from galloping and from wake-induced oscillation, but mainly is caused by Aeolian vibration. Fatigue occurs at support locations, suspension clamps, insulators, and dead ends. They also include damper and bundle conductor spacer clamps, hot-line taps, splices, and armour rod end clamps. The incidence of fatigue relative to the above locations is directly associated with the rigidity with which conductor motion is restrained. Fatigue of conductor strands is caused by the cyclic bending of the conductors where their motion is restrained. With increasing bending amplitude fatigue life decreases.

The complications of relating the measurable vibration of conductor to know the chance of fatigue of its strands is a complicated matter arising primarily from two facts. First, the stresses that cause the failures are complex and not related in a simple way to the gross motions of the conductor. Second, the failures are located on surface contact between components. Inspection and failure analysis of a large number of fatigue breaks from field and laboratory spans indicate that the fatigue always takes place where the broken strand was in contact with another strand or another related component. The stresses at these locations are combinations of static stresses due to conductor tension, bending, and the compressive force between the members.

Figure 3-6 Radiographic inspection procedure [2]

Figure 3-7 Prototype Electro-magneto-acoustic transducer (EMAT) device for detecting broken conductor strands [2]

3.3 Galloping

Since the time galloping of iced conductors was found, numerous research programs in the world have been done. Aimed to solve the problem and various devices and techniques have been developed to prevent or minimalism effect of galloping. Many methods were used to prevent galloping with mixed results. No practical protection method has been developed to prevent all types of galloping under any ice and wind conditions. Approach to this problem is in analytical way and with the growth of computer capability are many solutions of complex problem in the analysis of galloping behaviour. But even when all relevant parameters of weather and line construction are known, there are still areas of uncertainty and isn't possible to know exact behaviour.

Galloping is a low-frequency (0,1-1Hz), large amplitude (±0,1 times - ±1 times sag of the span), wind-induced vibration of both single or bundle conductors, with a single or a few loops of standing waves per span. This type of motion is caused by moderately strong, steady crosswind acting upon an asymmetrically iced conductor surface. This type of motion has major impact on the design of overhead lines and tower load. The space between lines has to be enough to prevent flashovers between lines, which are the most common effect of galloping. Large, repeated loads may cause bending of towers and cross arms.

There are two basic forms of galloping, standing waves and travelling waves, or a combination of them. From the beginning are waves tens of meters long, with amplitudes of a few centimetres. In the time, they grow in length and amplitude and can interact with one another to create standing waves. From several loops per span at the beginning will be later only few loops per span. Observed peak-to-peak amplitudes of galloping are often as great as the sag in the span and in case of short spans should be greater.

Typical conductor motions are vertical in galloping, but there is often motion in horizontal direction. These motions aren't often in phase, so the motions are elliptical.
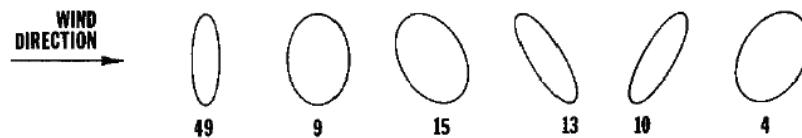
Figure 3-8 Percentage of observations of various galloping ellipse shapes and tilts [2]

Galloping caused various kinds of structural damage in overhead lines because of large forces that galloping motion applies to devices. Galloping causes damage to cross arms, insulators, towers, vibration dampers, and conductor strings. When galloping amplitudes are great enough, flashover can occur between phases or from phase to ground and it causes damage to the conductor.
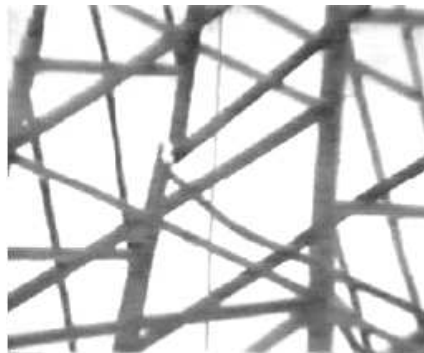
Figure 3-9 Damage due to galloping on towers [2]

Figure 3-10 Damage due to galloping on a string of suspension insulators [2]

Figure 3-11 Damage due to galloping on a triple bundle conductor in China [2]
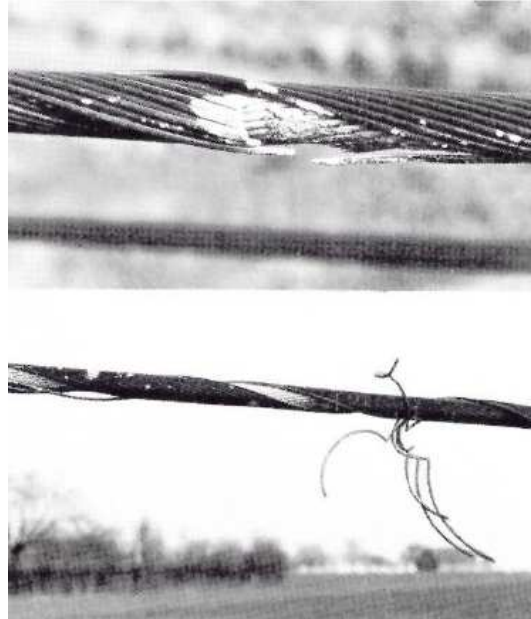
Figure 3-12 Broken strands resulting from short circuit due to two-phase fault induced by galloping [2]

3.4 Bundle Conductor Oscillations

Bundle conductor oscillation (or wake-induced oscillation), is another motion recognized as a problem in transmission lines of bundle conductors. It doesn't cause as serious of a problem like previous motions and damage had been limited to rapid wear in suspension hardware or fatigue of spacers or other accessories.
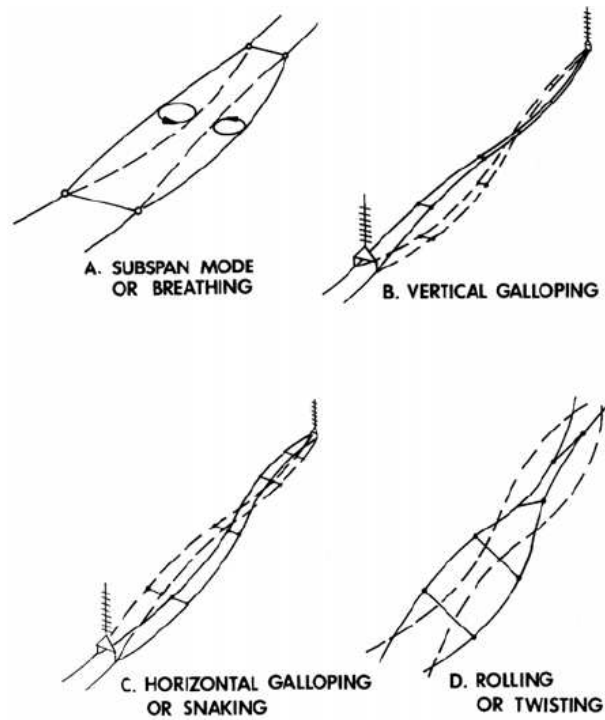
Figure 3-13 Classification of wake-induced motions [2]

Figure 3-14 Twin spacer-damper with cantilever clamps [2]

Figure 3-15 Triple spacer-damper with two articulations per arm and hinge type clamps [2]

Figure 3-16 Quad spacer-damper with elastomer-lined clamp and helical rod attachment [2]
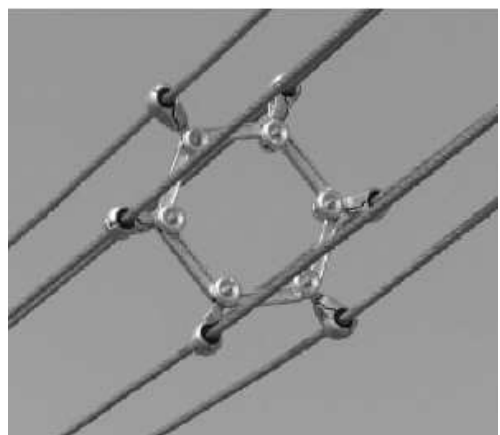
Figure 3-17 Six-bundle spacer-damper with rubber-lined clamps [2]

3.5 Other motions

Other types of motion:

- Short-Circuit Forces in Power Lines and Substations

- Bundle Conductor Rolling

- Ice and Snow Shedding

- Gust Response

- Vibration of Tower Members

- Noise from Overhead Lines

- Earthquake Effects on Overhead Conductors

- Corona Vibration

- Station Bus Vibration

3.5.1 Short-Circuit Forces in Power Lines and Substations

Forces generated by short-circuit are very important for high-voltage bundle conductor lines, medium-voltage distribution lines, and substations. For bundle conductor lines, during a fault, the sub conductors of the bundle move closer to each other due to strong attraction forces because of the very short distance between sub conductors.
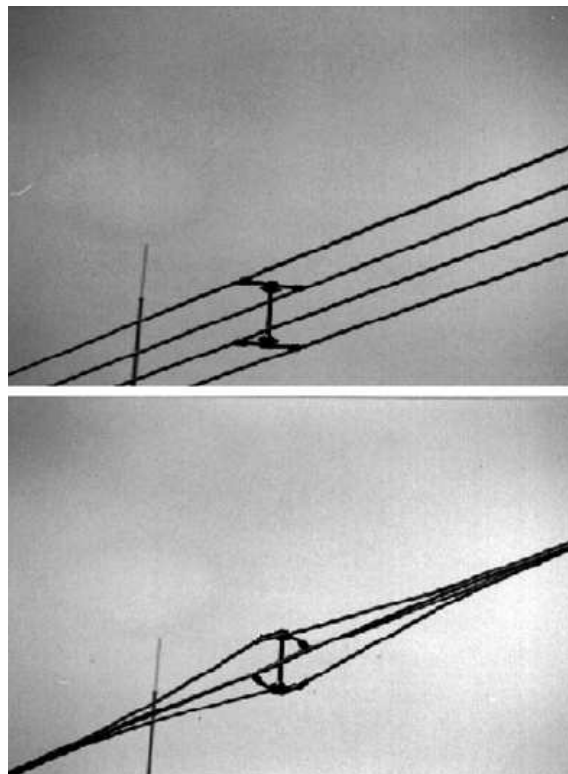
Figure 3-18 Short circuit test [2]

Figure 3-18 shows an example of quad bundle before and during short-circuit test at 50 kA, showing distortion of the sub conductors. One flexible spacer is at midspan. The sub conductor movements occur at very high acceleration. For example, a 40 kA fault on a twin bundle of 620

mm^2 conductor, with a separation of 40 cm, may have acceleration up to several tens of g, depending on the instantaneous current value.

Very large movements may be seen on distribution lines. Figure 3-19 shows the motion produced during testing on an actual line. This is from an actual three-phase short-circuit test on a 15-kV distribution line. The photo shows an instantaneous position of the conductors taken during the test. The fault current level was 3 kA.

Figure 3-19 Instantaneous position of the conductors taken during three-phase short-circuit test on 15-kV [2]

3.5.2 Ice and snow shedding

It is a natural process that occurs when accumulated ice is removed. Sudden ice or snow shedding from transmission lines may result in high-amplitude vibrations or jump of the conductor. Therefore is important in design of transmission line to predict both, the maximum jump height of the unloaded span and the maximum drop in the span that remains loaded to avoid flashover. As well, it is necessary to predict the maximum cable tension.
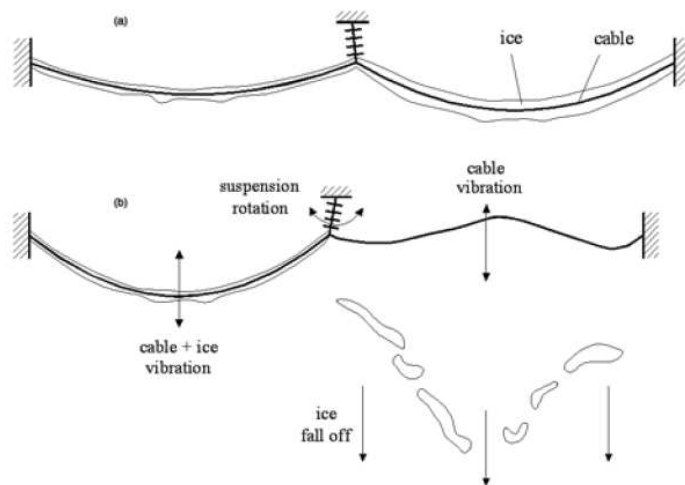
Figure 3-20 Ice shedding from one span and the resulting motions [2]

4 MEASURING DEVICES

In space there are 6 degrees of freedom. There are three rotations and three movements. If I need to know instantaneous position and orientation in space, I need to measure acceleration in three dimensions and angular velocity in three dimensions by 3D accelerometer and 3D gyroscope. From these values I am able to count position in case of known nine initial conditions as you can see from the equations below (in case that I have enough high sampling frequency to suppose constant discrete values of acceleration and angular velocity).

$$\mathbf{r}_{xyz} = \int \left(\int \mathbf{a}_{xyz} dt \right) dt = \int \left(\mathbf{a}_{xyz} \cdot t + \mathbf{v}_{0xyz} \right) dt = \frac{1}{2} \cdot \mathbf{a}_{xyz} \cdot t^2 + \mathbf{v}_{0xyz} \cdot t + \mathbf{r}_{0xyz} \qquad (4.1)$$

$$\varphi_{xyz} = \int \omega_{xyz} dt = \omega_{xyz} t + \varphi_{0xyz} \qquad (4.2)$$

4.1 Gyroscope

Gyroscope is an object formed in the shape of discs, but it can be any object. Necessary is to produce effective gyroscopic behaviour. Disc often have a large heavy ring because the mass should be as far away from the centre as possible. When the gyroscope isn't rotating it behaves like any other object, however when the gyroscope is rotating at high speed it has special behaviour by resisting movements in certain directions.
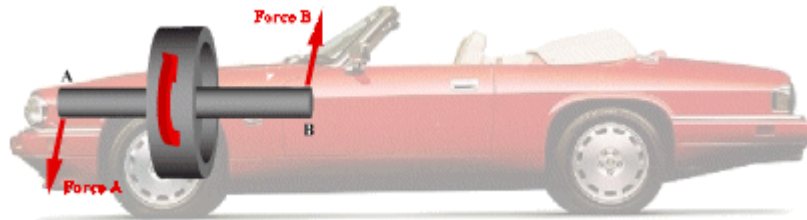
Figure 4-1 Engine of car like gyroscope [11]

Gyroscope contains large amounts of stored energy when it is rotating. Newton's first law of motion says, "Every object in a state of uniform motion tends to remain in that state of motion unless an external force is applied to it." It means that when I will apply force to gyroscope, the gyroscope will try to compensate because of this acting force.

Often the engine of cars behaves as a gyroscope because of its shape, mass and rotations. Let's have gyroscope/engine which is spinning at a high speed in a clockwise direction as seen on the picture above. When the car is turned to the right forces A and B are applied to the structure of the car forcing the front end of the car down and the back end up. If the car is turned to the left then the front end of the car is forced up and the back end forced down. If the gyroscope is spinning in the opposite direction then the reverse will happened.

However if the car was moved directly upwards, downwards, forwards, back-wards or side-to-side the gyroscope would not apply any extra forces. The gyroscope only applies extra forces when the car is moving at an angle. This effect is known as gyroscopic precession.
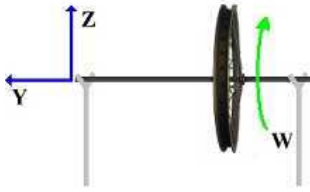
Figure 4-2 Gyroscope
principle [11]
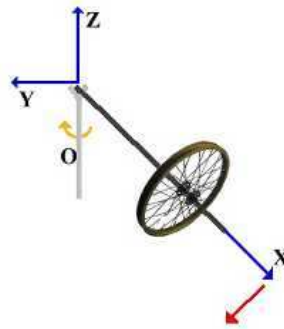
Figure 4-3 Gyroscope
principle [11]
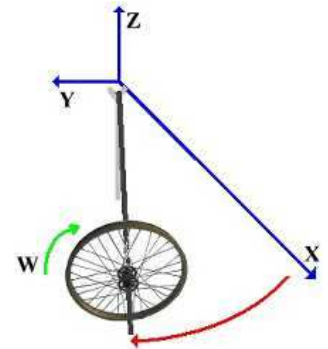
Figure 4-4 Gyroscope
principle [11]

The Figure 4-2 shows a bicycle wheel acting like a gyroscope being supported at both ends of the axle, if left this way the gyroscope would just slowly stop spinning. However if the right support is removed then gravity exerts a force pushing the right hand side of axle down. As described in earlier, gyroscopic precession will force the wheel to precess around its axis, as shown in Figure 4-3 and Figure 4-4 by the red arrows. The direction the precession takes depends on the rotational direction of the gyroscopes, shown in the diagram as green arrows. If the wheel is continuously unsupported then the wheel will continue to rotate around its axis.

It means that if I know angular velocity and initial condition of angle in one axis I can count instantaneous angle position. And if I have 3D gyroscope, I can know orientation in space on conditions of known three time derivations of angular velocities and three initial conditions of angles.

4.2 Accelerometer

An accelerometer is a device that measures the vibration, or acceleration of motion of a structure. The force caused by vibration or a change in motion (acceleration) causes the mass to "squeeze" the piezoelectric material which produces an electrical charge that is proportional to the force exerted upon it. Since the charge is proportional to the force, and the mass is a constant, then the charge is also proportional to the acceleration.

There are two types of piezoelectric accelerometers. The first type is a "high impedance" charge output accelerometer. In this type of accelerometer the piezoelectric crystal produces an electrical charge which is connected directly to the measurement devices.

The charge output measurement requires special equipment most commonly found in research facilities. This type of accelerometer is also used in high temperature applications (>120°C) where low impedance models can not be used.

The second type of accelerometer is a low impedance output accelerometer. A low impedance accelerometer has a charge accelerometer as its front end but has a tiny built-in micro-circuit and FET transistor that converts that charge into a low impedance voltage that can easily interface with standard devices. This type of accelerometer is commonly used in industry.

It means that if I know the acceleration and initial conditions of speed and position in one axle I can count instantaneous position. And if I have 3D accelerometer, I can know position in space on conditions of the known three instantaneous accelerations and the three initial conditions of speed and the three initial conditions of a position.

4.3 Devices in Ampacimon®

Here (in Ampacimon® module), are used MEMS sensors (accelerometers and gyroscopes). MEMS are not piezoelectric accelerometers and there is no rotating movement in MEMS gyroscopes.

Typical MEMS accelerometer is composed of movable proof mass with plates that is attached through a mechanical suspension system to a reference frame. Movable plates and fixed outer plates represent capacitors. The deflection of proof mass is measured using the capacitance difference. It is capacitance changes due to changes of distance between capacitor plates.

See [28] for understanding of MEMS sensors.

5 KALMAN FILTER

5.1 Example applications

An example application would be providing accurate continuously-updated information about the position and velocity of an object given only a sequence of observations about its position, each of which includes some error. It is used in a wide range of engineering applications from radar to computer vision. Kalman filtering is an important topic in control theory and control systems engineering.

For example, in a radar application, where one is interested in tracking a target, information about the location, speed, and acceleration of the target is measured with a great deal of corruption by noise at any time. The Kalman filter exploits the dynamics of the target, which govern its time evolution, to remove the effects of the noise and get a good estimate of the location of the target at the present time (filtering), at a future time (prediction), or at a time in the past (interpolation or smoothing). A simplified version of a Kalman filter is the alpha beta filter, still commonly used, which has static weighting constants instead of using co-variance matrices.

5.2 Naming and historical development

The filter is named after Rudolf E. Kalman, though Thorvald Nicolai Thiele and Peter Swerling actually developed a similar algorithm earlier. Stanley F. Schmidt is generally credited with developing the first implementation of a Kalman filter. It was during a visit of Kalman to the NASA Ames Research Center that he saw the applicability of his ideas to the problem of trajectory estimation for the Apollo program, leading to its incorporation in the Apollo navigation computer. The filter was developed in papers by Swerling (1958), Kalman (1960), and Kalman and Bucy (1961).

The filter is sometimes called Stratonovich-Kalman-Bucy filter because it is a special case of a more general, non-linear filter developed earlier by Ruslan L. Stratonovich. In fact, equations of the special case, linear filter appeared in these papers by Stratonovich that were published before summer 1960, when Kalman met with Stratonovich during a conference in Moscow.

In control theory, the Kalman filter is most commonly referred to as **linear quadratic estimation** (LQE).

A wide variety of Kalman filters have now been developed, from Kalman's original formulation, now called the *simple* Kalman filter, to Schmidt's *extended* filter, the *information* filter and a variety of *square-root* filters developed by Bierman, Thornton, and many others. Perhaps the most commonly used type of Kalman filter is the phase-locked loop now ubiquitous in radios, computers, and nearly any other type of video or communications equipment.

5.3 Underlying dynamic system model

Kalman filters are based on linear dynamical systems discretised in the time domain. They are modelled on a Markov chain built on linear operators perturbed by Gaussian noise. The state of the system is represented as a vector of real numbers. At each discrete time increment, a linear operator is applied to the state to generate the new state, with some noise mixed in, and optionally some information from the controls on the system if they are known. Then, another linear operator mixed with more noise generates the visible outputs from the hidden state. The Kalman filter may be regarded as analogous to the hidden Markov model, with the key difference that the

hidden state variables take values in a continuous space (as opposed to a discrete state space as in the hidden Markov model). Additionally, the hidden Markov model can represent an arbitrary distribution for the next value of the state variables, in contrast to the Gaussian noise model that is used for the Kalman filter. There is a strong duality between the equations of the Kalman Filter and those of the hidden Markov model. A review of this and other models is given in Roweis and Ghahramani (1999).

In order to use the Kalman filter to estimate the internal state of a process given only a sequence of noisy observations, one must model the process in accordance with the framework of the Kalman filter. This means specifying the matrices $\mathbf{F}_k$, $\mathbf{H}_k$, $\mathbf{Q}_k$, $\mathbf{R}_k$, and sometimes $\mathbf{B}_k$ for each time-step k as described below.
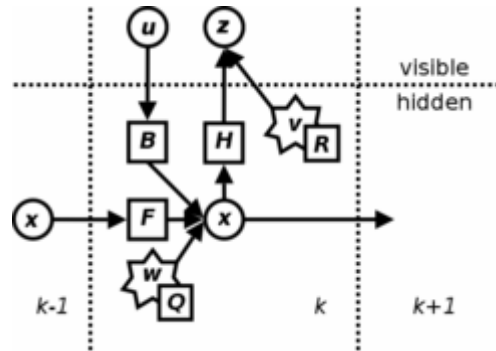
Figure 5-1 Model underlying the Kalman filter. [5]

Circles are vectors, squares are matrices, and stars represent Gaussian noise with the associated covariance matrix at the lower right.

The Kalman filter model assumes the true state at time k is evolved from the state at $(k-1)$ according to

$$\mathbf{x}_k = \mathbf{F}_k \cdot \mathbf{x}_{k-1} + \mathbf{B}_k \cdot \mathbf{u}_k + \mathbf{w}_k \tag{5.1}$$

where

- $\mathbf{F}_k$ is the state transition model which is applied to the previous state $\mathbf{x}_{k-1}$;

- $\mathbf{B}_k$ is the control-input model which is applied to the control vector $\mathbf{u}_k$;

- $\mathbf{w}_k$ is the process noise which is assumed to be drawn from a zero mean multivariate normal distribution with covariance $\mathbf{Q}_k$.

$$\mathbf{w}_k \quad N\left(0, \mathbf{Q}_k\right) \tag{5.2}$$

At time k an observation (or measurement) $\mathbf{z}_k$ of the true state $\mathbf{x}_k$ is made according to

$$\mathbf{z}_k = \mathbf{H}_k \cdot \mathbf{x}_k + \mathbf{v}_k \tag{5.3}$$

where $\mathbf{H}_k$ is the observation model which maps the true state space into the observed space and $\mathbf{v}_k$ is the observation noise which is assumed to be zero mean Gaussian white noise with covariance $\mathbf{R}_k$.

$$\mathbf{v}_k \quad N\left(0, \mathbf{R}_k\right) \tag{5.4}$$

The initial state, and the noise vectors at each step $\{\mathbf{x}_0, \mathbf{w}_1, ..., \mathbf{w}_k, \mathbf{v}_1 ... \mathbf{v}_k\}$ are all assumed to be mutually independent.

Many real dynamical systems do not exactly fit this model; however, because the Kalman filter is designed to operate in the presence of noise, an approximate fit is often good enough for the filter to be very useful. Variations on the Kalman filter described below allow richer and more sophisticated models.

5.4 The Kalman filter

The Kalman filter is a recursive estimator. This means that only the estimated state from the previous time step and the current measurement are needed to compute the estimate for the current state. In contrast to batch estimation techniques, no history of observations and/or estimates is required. It is unusual in being purely a time domain filter; most filters (for example, a low-pass filter) are formulated in the frequency domain and then transformed back to the time domain for implementation. In what follows, the notation $\hat{\mathbf{x}}_{n|m}$, represents the estimate of $\mathbf{x}$, at time n given observations up to, and including time m.

The state of the filter is represented by two variables:

- $\hat{\mathbf{x}}_{k|k}$, the estimate of the state at time k given observations up to and including time k;

- $\mathbf{P}_{k|k}$, the error covariance matrix (a measure of the estimated accuracy of the state estimate).

The Kalman filter has two distinct phases: **Predict** and **Update**. The predict phase uses the state estimate from the previous time step to produce an estimate of the state at the current time step. In the update phase, measurement information at the current time step is used to refine this prediction to arrive at a new, more accurate state estimate, again for the current time step.

5.4.1 Predict

Predicted state

$$\hat{\mathbf{x}}_{k|k-1} = \mathbf{F}_k \cdot \hat{\mathbf{x}}_{k-1|k-1} + \mathbf{B}_{k-1} \cdot \mathbf{u}_{k-1} \tag{5.5}$$

Predicted estimate covariance

$$\mathbf{P}_{k|k-1} = \mathbf{F}_k \cdot \mathbf{P}_{k-1|k-1} \cdot \mathbf{F}_k^T + \mathbf{Q}_{k-1} \tag{5.6}$$

5.4.2 Update

Innovation or measurement residual

$$\tilde{\mathbf{y}}_k = \mathbf{z}_k - \mathbf{H}_k \cdot \hat{\mathbf{x}}_{k|k-1} \tag{5.7}$$

Innovation (or residual) covariance

$$\mathbf{S}_k = \mathbf{H}_k \cdot \mathbf{P}_{k|k-1} \cdot \mathbf{H}_k^T + \mathbf{R}_k \tag{5.8}$$

Optimal Kalman gain

$$\mathbf{K}_k = \mathbf{P}_{k|k-1} \cdot \mathbf{H}_k^T \cdot \mathbf{S}_k^{-1} \tag{5.9}$$

Updated state estimate

$$\hat{\mathbf{x}}_{k|k} = \hat{\mathbf{x}}_{k|k-1} + \mathbf{K}_k \cdot \tilde{\mathbf{y}}_k \tag{5.10}$$

Updated estimate covariance

$$\mathbf{P}_{k|k} = \left(I - \mathbf{K}_k \cdot \mathbf{H}_k \right) \cdot \mathbf{P}_{k|k-1} \tag{5.11}$$

The formula for the updated estimate covariance above is only valid for the optimal Kalman gain. Usage of other gain values requires a more complex formula found in the *derivations* section.
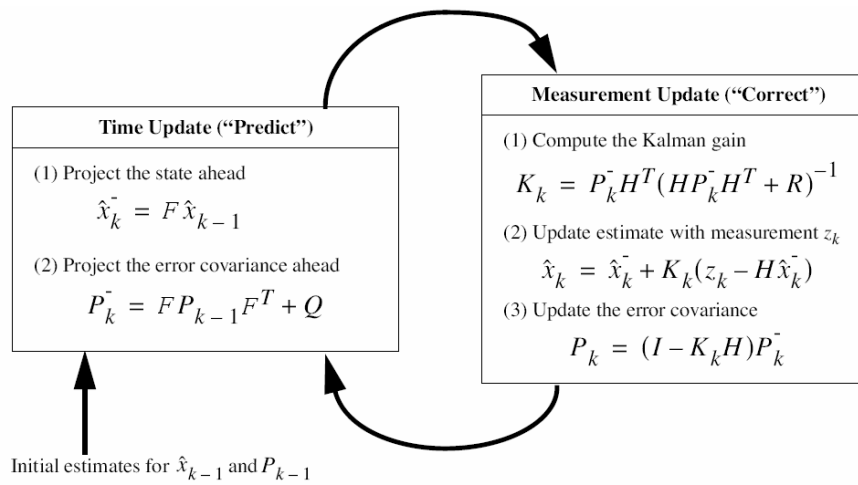

Time Update ("Predict")

(1) Project the state ahead

$$\hat{x}_k^- = F \hat{x}_{k-1}$$

(2) Project the error covariance ahead

$$P_k^- = F P_{k-1} F^T + Q$$

Measurement Update ("Correct")

(1) Compute the Kalman gain

$$K_k = P_k^- H^T (H P_k^- H^T + R)^{-1}$$

(2) Update estimate with measurement z_k

$$\hat{x}_k = \hat{x}_k^- + K_k (z_k - H \hat{x}_k^-)$$

(3) Update the error covariance

$$P_k = (I - K_k H) P_k^-$$

Initial estimates for $\hat{x}_{k-1}$ and P_{k-1}

Figure 5-2 How Kalman filter works [7]

5.4.3 Invariants

If the model is accurate, and the values for $\hat{x}_{0|0}$ and $\mathbf{P}_{0|0}$ accurately reflect the distribution of the initial state values, then the following invariants are preserved: all estimates have mean error equal to zero.

$$E\left[\mathbf{x}_k - \hat{\mathbf{x}}_{k|k}\right] = E\left[\mathbf{x}_k - \hat{\mathbf{x}}_{k|k-1}\right] = 0 \tag{5.12}$$

$$E\left[\tilde{\mathbf{y}}_k\right] = 0 \tag{5.13}$$

where E[ξ] is the expected value of ξ, and covariance matrices accurately reflect the covariance of estimates

$$\mathbf{P}_{k|k} = \mathrm{cov}\left(\mathbf{x}_k - \hat{\mathbf{x}}_{k|k}\right) \tag{5.14}$$

$$\mathbf{P}_{k|k-1} = \mathrm{cov}\left(\mathbf{x}_k - \hat{\mathbf{x}}_{k|k-1}\right) \tag{5.15}$$

$$\mathbf{S}_k = \mathrm{cov}\left(\tilde{\mathbf{y}}_k\right) \tag{5.16}$$

5.5 Examples

Consider a truck on perfectly frictionless, infinitely long straight rails. Initially the truck is stationary at position 0, but it is buffeted this way and that by random acceleration. We measure the position of the truck every Δt seconds, but these measurements are imprecise; we want to maintain a model of where the truck is and what its velocity is. We show here how we derive the model from which we create our Kalman filter.

There are no controls on the truck, so we ignore $\mathbf{B}_k$ and $\mathbf{u}_k$. Since $\mathbf{F}$, $\mathbf{H}$, $\mathbf{R}$ and $\mathbf{Q}$ are constant, their time indices are dropped.

The position and velocity of the truck is described by the linear state space

$$\mathbf{x}_k = \begin{pmatrix} x \\ \dot{x} \end{pmatrix} \tag{5.17}$$

Where is the velocity, that is, the derivative of position with respect to time.

We assume that between the $(k-1)^{\text{th}}$ and k^{th} time step the truck undergoes a constant acceleration of a_k that is normally distributed, with mean 0 and standard deviation σ_a. From Newton's laws of motion we conclude that

$$\mathbf{x}_k = \mathbf{F} \cdot \mathbf{x}_{k-1} + \mathbf{G} \cdot a_k \tag{5.18}$$

where

$$\mathbf{F} = \begin{pmatrix} 1 & \Delta t \\ 0 & 1 \end{pmatrix} \tag{5.19}$$

and

$$\mathbf{G} = \begin{pmatrix} \dfrac{\Delta t^2}{2} \\ \Delta t \end{pmatrix} \tag{5.20}$$

We find that

$$\mathbf{Q} = \text{cov}(\mathbf{G} \cdot a) = E\left[(\mathbf{G} \cdot a) \cdot (\mathbf{G} \cdot a)^T\right] = \mathbf{G} \cdot E\left[a^2\right] \cdot \mathbf{G}^T = \mathbf{G}\left[\sigma_a^2\right] \cdot \mathbf{G}^T = \sigma_a^2 \cdot \mathbf{G} \cdot \mathbf{G}^T \tag{5.21}$$

(since σ_a is a scalar).

At each time step, a noisy measurement of the true position of the truck is made. Let us suppose the noise is also normally distributed, with mean 0 and standard deviation σ_z.

$$\mathbf{z}_k = \mathbf{H} \cdot \mathbf{x}_k + \mathbf{v}_k \tag{5.22}$$

where

$$\mathbf{H} = \begin{pmatrix} 1 & 0 \end{pmatrix} \tag{5.23}$$

and

$$\mathbf{R} = E\left(\mathbf{v}_k \cdot \mathbf{v}_k^T\right) = \left(\sigma_z^2\right) \tag{5.24}$$

We know the initial starting state of the truck with perfect precision, so we initialize

$$\hat{\mathbf{x}}_{0|0} = \begin{pmatrix} 0 \\ 0 \end{pmatrix} \tag{5.25}$$

and to tell the filter that we know the exact position, we give it a zero covariance matrix:

$$\mathbf{P}_{0|0} = \begin{pmatrix} 0 & 0 \\ 0 & 0 \end{pmatrix} \tag{5.26}$$

If the initial position and velocity are not known perfectly the covariance matrix should be initialized with a suitably large number, say *B*, on its diagonal.

$$\mathbf{P}_{0|0} = \begin{pmatrix} B & 0 \\ 0 & B \end{pmatrix} \tag{5.27}$$

The filter will then prefer the information from the first measurements over the information already in the model.

5.6 Derivations

5.6.1 Deriving the posterior estimate covariance matrix

Starting with our invariant on the error covariance $\mathbf{P}_{k|k}$ as above

$$\mathbf{P}_{k|k} = \mathrm{cov}\left(\mathbf{x}_k - \hat{\mathbf{x}}_{k|k}\right) \tag{5.28}$$

substitute in the definition of $\hat{\mathbf{x}}_{k|k}$

$$\mathbf{P}_{k|k} = \mathrm{cov}\left(\mathbf{x}_k - \left(\hat{\mathbf{x}}_{k|k-1} + \mathbf{K}_k \cdot \tilde{\mathbf{y}}_k\right)\right) \tag{5.29}$$

and substitute $\tilde{\mathbf{y}}_k$

$$\mathbf{P}_{k|k} = \mathrm{cov}\left(\mathbf{x}_k - \left(\hat{\mathbf{x}}_{k|k-1} + \mathbf{K}_k \cdot \left(\mathbf{z}_k - \mathbf{H}_k \cdot \hat{\mathbf{x}}_{k|k-1}\right)\right)\right) \tag{5.30}$$

and $\mathbf{z}_k$

$$\mathbf{P}_{k|k} = \mathrm{cov}\left(\mathbf{x}_k - \left(\hat{\mathbf{x}}_{k|k-1} + \mathbf{K}_k \cdot \left(\mathbf{H}_k \cdot \mathbf{x}_k + \mathbf{v}_k - \mathbf{H}_k \cdot \hat{\mathbf{x}}_{k|k-1}\right)\right)\right) \tag{5.31}$$

and by collecting the error vectors we get

$$\mathbf{P}_{k|k} = \mathrm{cov}\left(\left(I - \mathbf{K}_k \cdot \mathbf{H}_k\right) \cdot \left(\mathbf{x}_k - \hat{\mathbf{x}}_{k|k-1}\right) - \mathbf{K}_k \cdot \mathbf{v}_k\right) \tag{5.32}$$

Since the measurement error $\mathbf{v}_k$ is uncorrelated with the other terms, this becomes

$$\mathbf{P}_{k|k} = \mathrm{cov}\left(\left(I - \mathbf{K}_k \cdot \mathbf{H}_k\right) \cdot \left(\mathbf{x}_k - \hat{\mathbf{x}}_{k|k-1}\right)\right) + \mathrm{cov}\left(\mathbf{K}_k \cdot \mathbf{v}_k\right) \tag{5.33}$$

by the properties of vector covariance this becomes

$$\mathbf{P}_{k|k} = \left(I - \mathbf{K}_k \cdot \mathbf{H}_k\right) \cdot \mathrm{cov}\left(\mathbf{x}_k - \hat{\mathbf{x}}_{k|k-1}\right) \cdot \left(I - \mathbf{K}_k \cdot \mathbf{H}_k\right)^T + \mathbf{K}_k \cdot \mathrm{cov}\left(\mathbf{v}_k\right) \cdot \mathbf{K}_k^T \tag{5.34}$$

which, using our invariant on $\mathbf{P}_{k|k-1}$ and the definition of $\mathbf{R}_k$ becomes

$$\mathbf{P}_{k|k} = \left(I - \mathbf{K}_k \cdot \mathbf{H}_k\right) \cdot \mathbf{P}_{k|k-1} \cdot \left(I - \mathbf{K}_k \cdot \mathbf{H}_k\right)^T + \mathbf{K}_k \cdot \mathbf{R}_k \cdot \mathbf{K}_k^T \tag{5.35}$$

This formula (sometimes known as the "**Joseph form**" of the covariance update equation) is valid no matter what the value of $\mathbf{K}_k$. It turns out that if $\mathbf{K}_k$ is the optimal Kalman gain, this can be simplified further as shown below.

5.6.2 Kalman gain derivation

The Kalman filter is a minimum mean-square error estimator. The error in the posterior state estimation is

$$\mathbf{x}_k - \hat{\mathbf{x}}_{k|k} \tag{5.36}$$

We seek to minimize the expected value of the square of the magnitude of this vector, $E\left(\left|\mathbf{x}_k - \hat{\mathbf{x}}_{k|k}\right|^2\right)$. This is equivalent to minimizing the trace of the posterior estimate covariance matrix $\mathbf{P}_{k|k}$. By expanding out the terms in the equation above and collecting, we get:

$$\begin{aligned} \mathbf{P}_{k|k} &= \mathbf{P}_{k|k-1} - \mathbf{K}_k \cdot \mathbf{H}_k \cdot \mathbf{P}_{k|k-1} - \mathbf{P}_{k|k-1} \cdot \mathbf{H}_k^T \cdot \mathbf{K}_k^T + \mathbf{K}_k \cdot \left(\mathbf{H}_k \cdot \mathbf{P}_{k|k-1} \cdot \mathbf{H}_k^T + \mathbf{R}_k\right) \cdot \mathbf{K}_k^T = \\ &= \mathbf{P}_{k|k-1} - \mathbf{K}_k \cdot \mathbf{H}_k \cdot \mathbf{P}_{k|k-1} - \mathbf{P}_{k|k-1} \cdot \mathbf{H}_k^T \cdot \mathbf{K}_k^T + \mathbf{K}_k \cdot \mathbf{S}_k \cdot \mathbf{K}_k^T \end{aligned} \tag{5.37}$$

The trace is minimized when the matrix derivative is zero:

$$\frac{\delta \, \mathrm{tr}\left(\mathbf{P}_{k|k}\right)}{\delta \mathbf{K}_k} = -2 \cdot \left(\mathbf{H}_k \cdot \mathbf{P}_{k|k-1}\right)^T + 2 \cdot \mathbf{K}_k \cdot \mathbf{S}_k = 0 \tag{5.38}$$

Solving this for $\mathbf{K}_k$ yields the Kalman gain:

$$\mathbf{K}_k \cdot \mathbf{S}_k = \left(\mathbf{H}_k \cdot \mathbf{P}_{k|k-1}\right)^T = \mathbf{P}_{k|k-1} \cdot \mathbf{H}_k^T \tag{5.39}$$

$$\mathbf{K}_k = \mathbf{P}_{k|k-1} \cdot \mathbf{H}_k^T \cdot \mathbf{S}_k^{-1} \tag{5.40}$$

This gain, which is known as the *optimal Kalman gain*, is the one that yields MMSE estimates when used.

5.6.3 Simplification of the posterior error covariance formula

The formula used to calculate the posterior error covariance can be simplified when the Kalman gain equals the optimal value derived above. Multiplying both sides of our Kalman gain formula on the right by $\mathbf{S}_k \mathbf{K}_k^T$, it follows that

$$\mathbf{K}_k \cdot \mathbf{S}_k \cdot \mathbf{K}_k^T = \mathbf{P}_{k|k-1} \cdot \mathbf{H}_k^T \cdot \mathbf{K}_k^T \tag{5.41}$$

Referring back to our expanded formula for the posterior error covariance,

$$\mathbf{P}_{k|k} = \mathbf{P}_{k|k-1} - \mathbf{K}_k \cdot \mathbf{H}_k \cdot \mathbf{P}_{k|k-1} - \mathbf{P}_{k|k-1} \cdot \mathbf{H}_k^T \cdot \mathbf{K}_k^T + \mathbf{K}_k \cdot \mathbf{S}_k \cdot \mathbf{K}_k^T \tag{5.42}$$

we find the last two terms cancel out, giving

$$\mathbf{P}_{k|k} = \mathbf{P}_{k|k-1} - \mathbf{K}_k \cdot \mathbf{H}_k \cdot \mathbf{P}_{k|k-1} = \left(I - \mathbf{K}_k \cdot \mathbf{H}_k \right) \cdot \mathbf{P}_{k|k-1} \tag{5.43}$$

This formula is computationally cheaper and thus nearly always used in practice, but is only correct for the optimal gain. If arithmetic precision is unusually low causing problems with numerical stability, or if a non-optimal Kalman gain is deliberately used, this simplification cannot be applied; the posterior error covariance formula as derived above must be used.

5.7 Relationship to the digital filter

The Kalman filter can be regarded as an adaptive low-pass infinite impulse response digital filter, with cut-off frequency depending on the ratio between the process and measurement (or observation) noise, as well as the estimate covariance. Frequency response is, however, rarely of interest when designing state estimators such as the Kalman Filter, whereas for digital filters such as IIR and FIR filters, frequency response is usually of primary concern. For the Kalman Filter, the important goal is how accurate the filter is, and this is most often decided based on empirical Monte Carlo simulations, where "truth" (the true state) is known.

6 2D MOVEMENT RECONSTRUCTION IN EXAMPLE

This chapter will take care how reproduce movement in 2D, based on measurements from 2D accelerometer and rated gyroscope. The aim will be to apply movement with device on known path and reproduce the movement using Kalman filtering on it and compare real path with non-filtered observed path and filtered path. Values aren't coming from measurement, they are fictitious!

6.1 Counting the path

Table 6-1 Known data

f	sampling frequency	200	Hz
$\mathbf{g}$	acceleration due to gravity	$\begin{pmatrix} 0 \\ -9.81 \end{pmatrix}$	$m \cdot s^{-2}$
$\mathbf{ag}_r$	matrix of measured accelerations	$\begin{pmatrix} a_{x1} & a_{x2} & a_{xm} & a_{xn} \\ a_{y1} & a_{y2} & a_{ym} & a_{yn} \end{pmatrix}$	$m \cdot s^{-2}$
$\boldsymbol{\omega}$	matrix of measured angular velocities	$\begin{pmatrix} \omega_1 & \omega_2 & \cdots \omega_m & \omega_n \end{pmatrix}$	$rad \cdot s^{-1}$

Table 6-2 Initialisation

r_{x0}	position in "x" axis	0	m
r_{y0}	position in "y" axis	0	m
v_{x0}	speed in "x" axis	-10	$m \cdot s^{-1}$
v_{y0}	speed in "y" axis	-2	$m \cdot s^{-1}$
φ_0	angle of rotation	0	rad

Time step dt :

$$dt = \frac{1}{f} \tag{6.1}$$
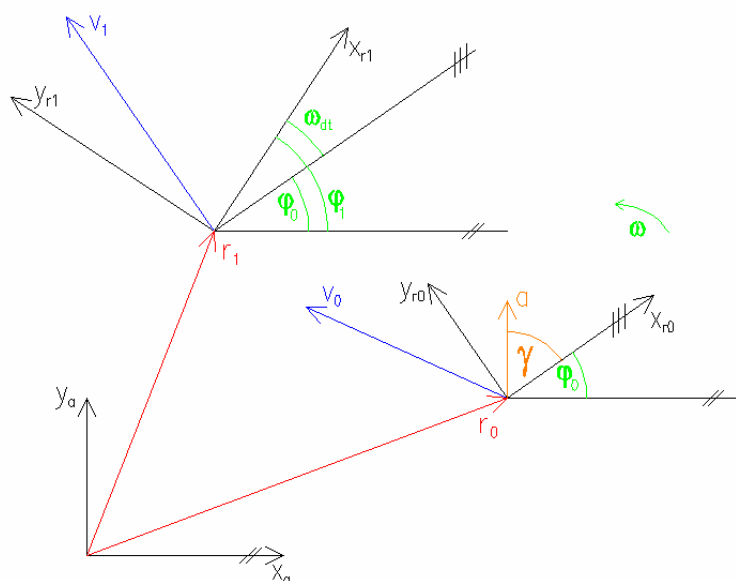
Figure 6-1 2D movement

Angle γ:

$$\gamma_1 = \arctan \frac{ag_{ry1}}{ag_{rx1}} \tag{6.2}$$

Angle φ:

$$\varphi_1 = \varphi_0 + \omega_1 \cdot dt \tag{6.3}$$

Relative acceleration ag_r divided to absolute axes is ag:

$$ag_{x1} = \sqrt{\left(ag_{rx1}^2 + ag_{ry1}^2\right)} \cdot \cos\left(\varphi_1 + \gamma_1\right)$$
$$ag_{y1} = \sqrt{\left(ag_{rx1}^2 + ag_{ry1}^2\right)} \cdot \cos\left(\varphi_1 + \gamma_1 - 0,5 \cdot \pi\right) \tag{6.4}$$

Without acceleration due to gravity is acceleration causing movement in absolute axes $\mathbf{a}$:

$$\mathbf{a}_1 = \mathbf{ag}_1 - \mathbf{g} \tag{6.5}$$

Absolute speed $\mathbf{v}$:

$$\mathbf{v}_1 = \mathbf{a}_1 \cdot dt + \mathbf{v}_0 \tag{6.6}$$

Positions $\mathbf{r}_c$:

$$\mathbf{r}_{c,1} = 0,5 \cdot \mathbf{a}_1 \cdot dt^2 + \mathbf{v}_0 \cdot dt + \mathbf{r}_{c,0} \tag{6.7}$$

6.2 Filtering the path

Table 6-3 Input data

Q	process noise matrix	$C^* \cdot \begin{pmatrix} 1 & 0 & 0 & 0 & 0 & 0 \\ 0 & 1 & 0 & 0 & 0 & 0 \\ 0 & 0 & 1 & 0 & 0 & 0 \\ 0 & 0 & 0 & 1 & 0 & 0 \\ 0 & 0 & 0 & 0 & 1 & 0 \\ 0 & 0 & 0 & 0 & 0 & 1 \end{pmatrix}$
R	measurement noise matrix	$D^* \cdot \begin{pmatrix} 1 & 0 \\ 0 & 1 \end{pmatrix}$
F	model matrix	$\begin{pmatrix} 1 & 0 & dt & 0 & 0.5 \cdot dt^2 & 0 \\ 0 & 1 & 0 & dt & 0 & 0.5 \cdot dt^2 \\ 0 & 0 & 1 & 0 & dt & 0 \\ 0 & 0 & 0 & 1 & 0 & dt \\ 0 & 0 & 0 & 0 & 1 & 0 \\ 0 & 0 & 0 & 0 & 0 & 1 \end{pmatrix}$

H	observation model	$\begin{pmatrix} 0 & 0 & 0 & 0 & 1 & 0 \\ 0 & 0 & 0 & 0 & 0 & 1 \end{pmatrix}$

Table 6-4 Initialisation

$\mathbf{P}_{0\|0}$	estimate covariance	$B^* \cdot \begin{pmatrix} 1 & 0 & 0 & 0 & 0 & 0 \\ 0 & 1 & 0 & 0 & 0 & 0 \\ 0 & 0 & 1 & 0 & 0 & 0 \\ 0 & 0 & 0 & 1 & 0 & 0 \\ 0 & 0 & 0 & 0 & 1 & 0 \\ 0 & 0 & 0 & 0 & 0 & 1 \end{pmatrix}$
$\hat{\mathbf{x}}_{0\|0}$	state estimate	$\begin{pmatrix} r_{x0} \\ r_{y0} \\ v_{x0} \\ v_{y0} \\ a_{x1} \\ a_{y1} \end{pmatrix}$

*Coefficients B, C, D will be found by filter tuning.

6.2.1 Kalman filter

Now is applied algorithm shown in Figure 5-2. Or you can see 5.4 The Kalman filter, 5.4.1 Predict and 5.4.2 Update.

Matrix of filtered positions $\mathbf{r}_f$:

$$\mathbf{r}_{f,k} = \hat{\mathbf{x}}_{k|k} \tag{6.8}$$

6.2.2 Filter tuning

Let's suppose that we had noisy two-row matrix of acceleration and vector of angular velocity. When we used some coefficients for drawing the filtered path, now we can tune the filter by slider.
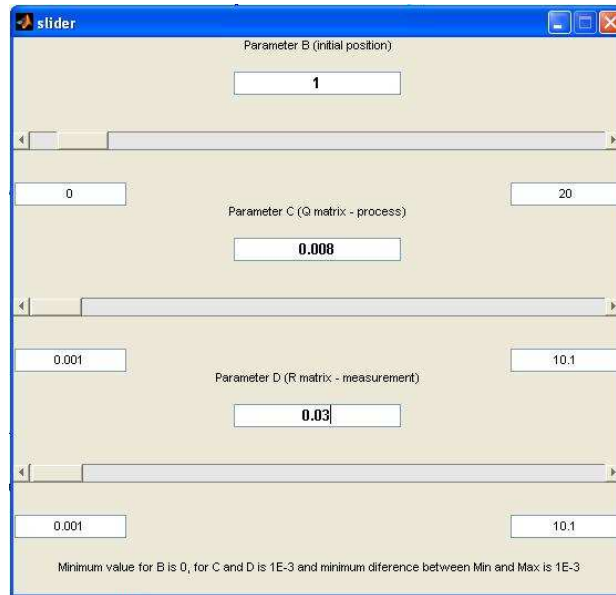
Figure 6-2 Slider for filter tuning

So less is B parameter, so better we know the initial position. When B is equal to zero, we know the exact initial position. So less is C parameter so better is system predictable and so less is D parameter so bigger is measurement valuable. The slider has 100 steps and minimum and maximum values are freely changeable. But minimum value for C and D parameter is limited to 0.001. And minimum difference between minimal and maximum value is limited to 0.001.

6.2.3 Results

Finally were found constants B=1, C=0.008 and D=0.03. Non filtered and filtered path could be seen in Figure 6-3. By blue colour is drawn non filtered path; by red colour is drawn filtered path with cyan prediction and magenta correction.
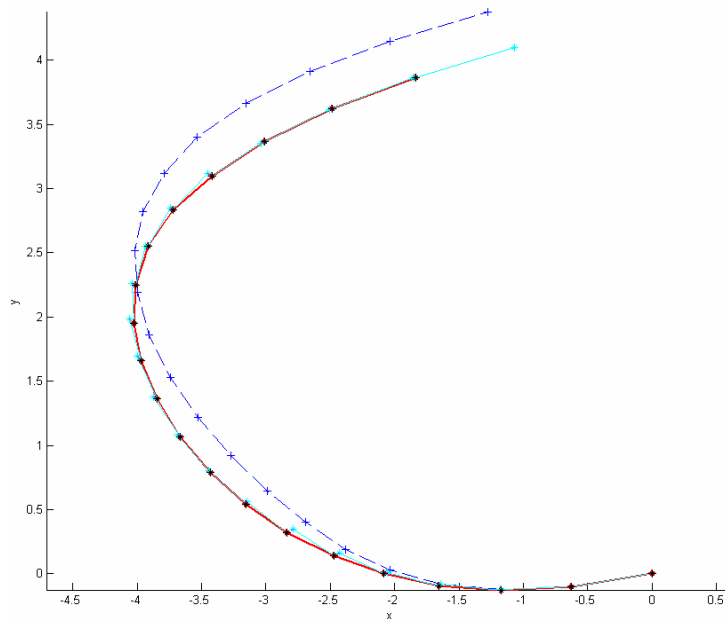
Figure 6-3 2D movement

M-files eventually other input data are on enclosed CD in directory - Movement_20Values.

7 VERTICAL MOVEMENT RECONSTRUCTION
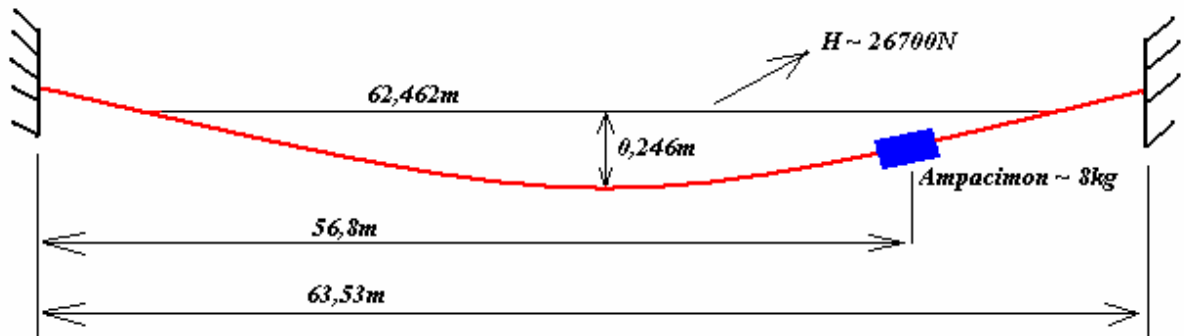
Figure 7-1 Test span in Canada

In Canada there is a test span where Ampacimon team to use Ampacimon device to measure in case of different movements. I am interested in movement when was Ampacimon device moved down by hands and released. Details of test span are in Figure 7-1 and in Table 7-1.

Table 7-1 Parameters of test span

Number of strands – aluminium/steel	54/7	-
Total diameter	26,3	mm
Mass per unit length	1,369	kg/m
Rated strength	117,2	kN
Aluminium strand diameter	2,9	mm
Aluminium area	362,6	mm^2
Steel strand diameter	2,9	mm
Steel area	47	mm^2
Module of elasticity	68,3	GPa
Dilatation coefficient	19,3	10^{-6}/°C

7.1 Observed data

For the measurement were used two accelerometers Y1 and Y3 in opposite directions. Calibration and offset were done. Final acceleration for movement reconstruction was count like (Y1-Y3)/2; acceleration due to gravity was subtracted. In theoretical way measurement from Y1 and Y3 should be the same with opposite sign and (Y1-Y3)/2 should be equal to Y1 as to –Y3. And (Y1+Y3)/2 should be equal to zero. In the real world it is different and will be shown below. Sampling frequency is 200Hz; time of one step is 5ms. No data from gyroscope were used in this experiment.
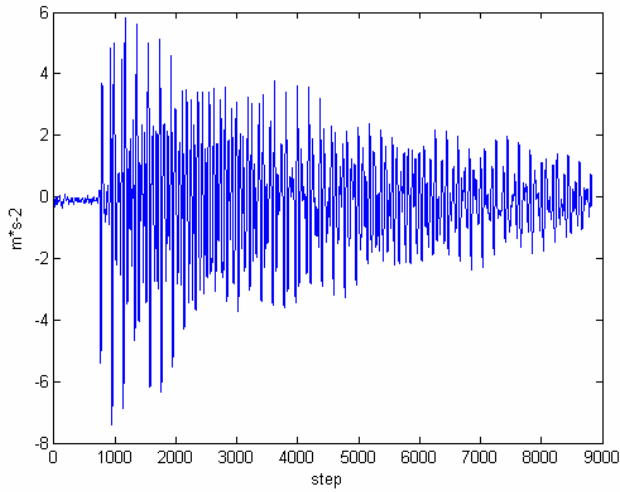
Figure 7-2 observed from Y1
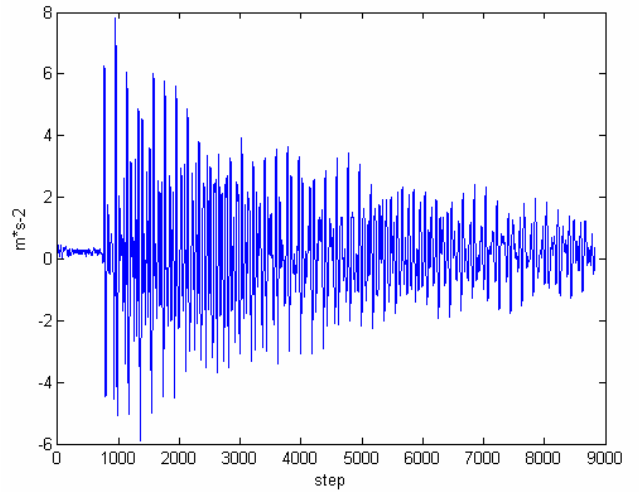
Figure 7-3 observed from Y3
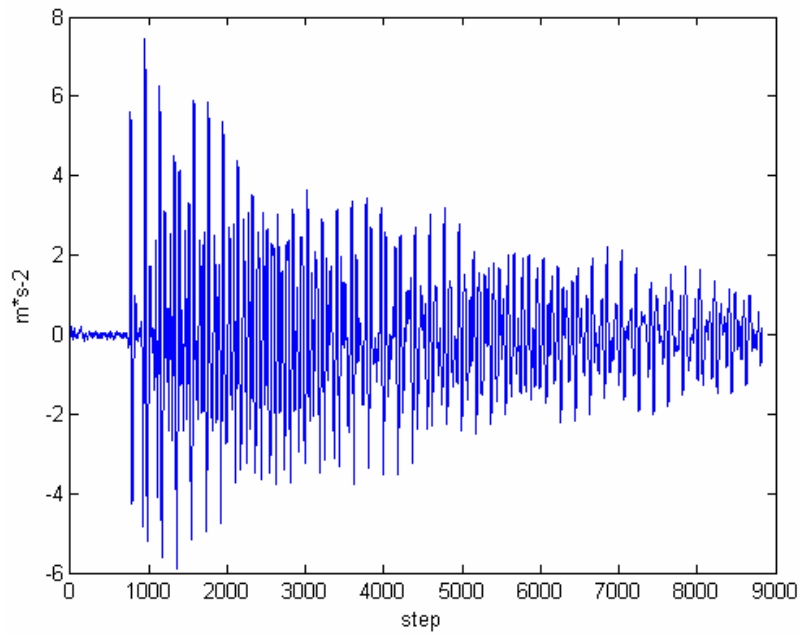
Figure 7-4 Final acceleration
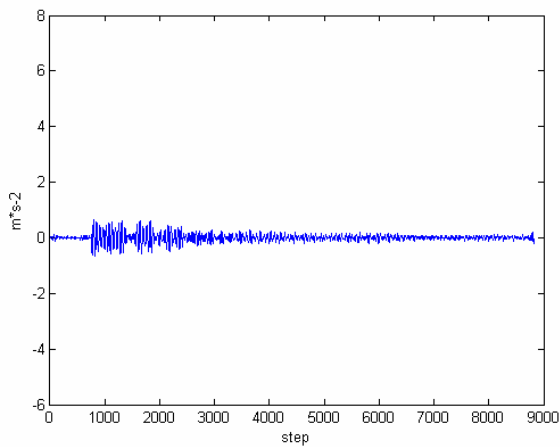
Figure 7-5 noise of meas. - (Y1+Y3)/2
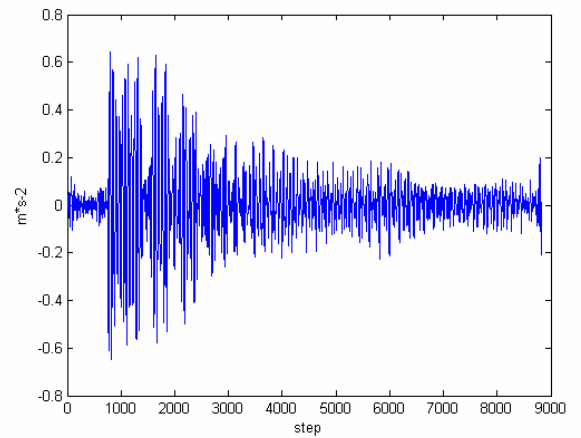
Figure 7-6 noise of meas. - (Y1+Y3)/2 in detail

7.2 Signal processing of observed measurement

Because of serious noise in measurement and even in process, I will be interested only in first few seconds of reproducing the path and it is enough for the final application. I suppose initial position approximately 6cm (it is a choice – I is not critical point) below steady state and initial velocity equal to zero.
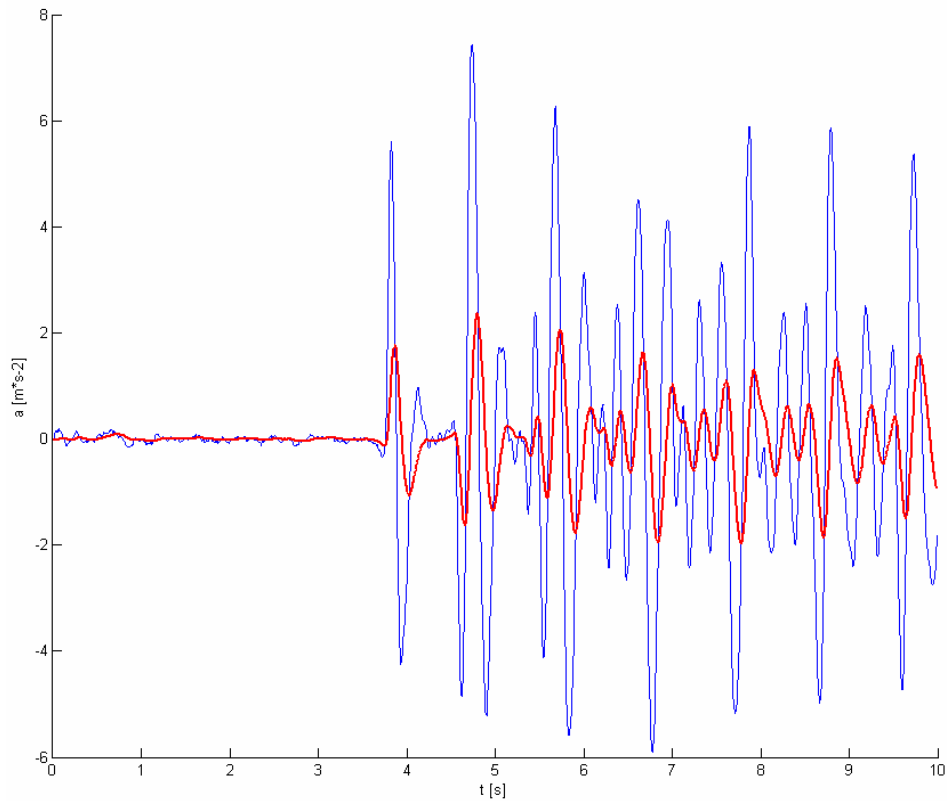
Figure 7-7 Measured (blue) and filtered (red) acceleration by Kalman filter
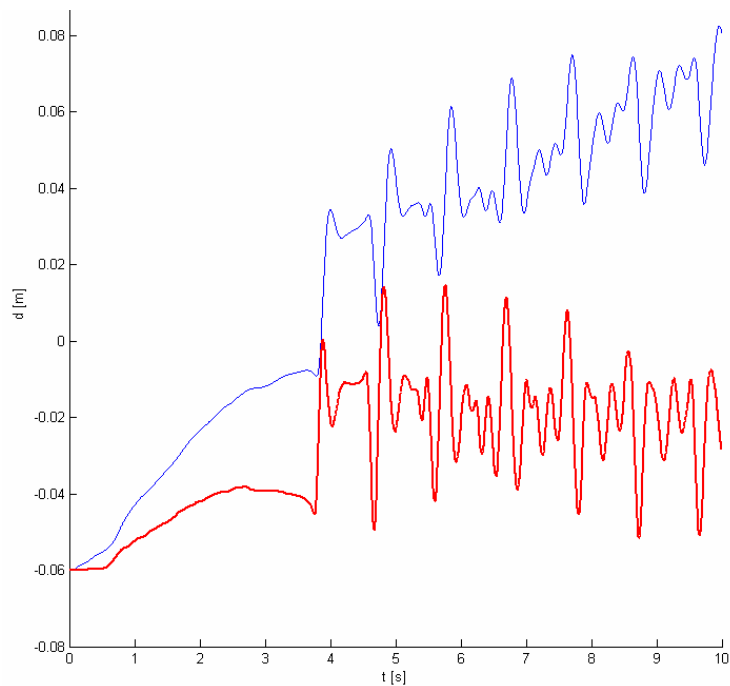
Figure 7-8 Non-filtered observed (blue) and filtered (red) position by Kalman filter

Due to the fact that I suppose initial velocity to zero, but it should be a little bit more than zero and due to the fact that each step used values from previous step and actual values are never corrected by other external system is in Figure 7-8 shift of position. It is impossible to reconstruct signal only from known accelerations.

M-files eventually other input data are on enclosed CD in directory - Movement_CA.

7.3 Signal processing of acceleration observed from model of span

By the method of finite elements is possible to have model of the span mentioned before and do all experiments on computer to verify truth of results. Even if is the measurement of acceleration very noisy and I want to verify algorithm for movement reproducing, it is possible to check it.

Details:

- number of element : 426

- time integration : automatic time integration (not fixed time step, adapted variable time step)

- excitation: applied constant force 250N aligned with gravity (vertical force downwards) during 4 seconds (between t=2s and t=6s).
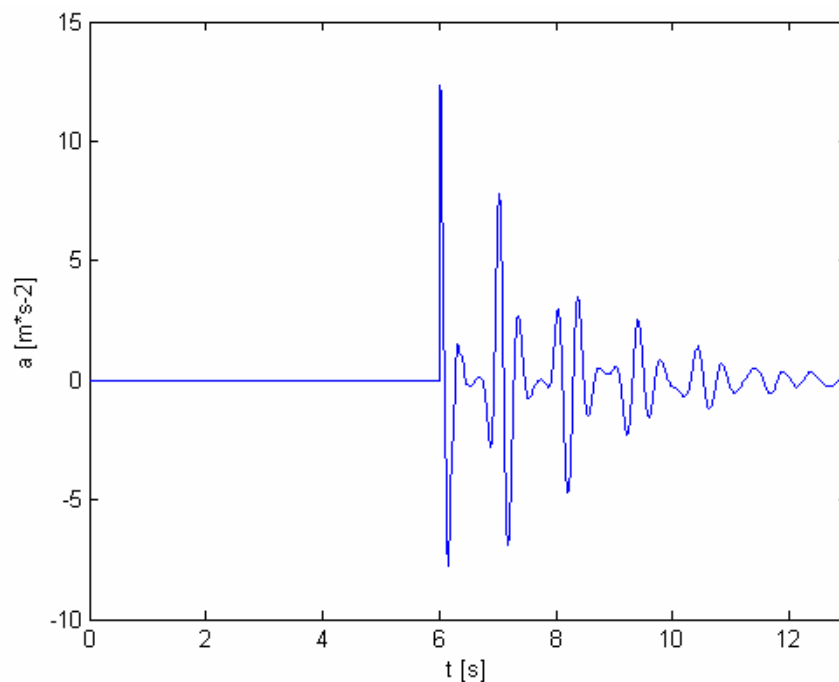
Figure 7-9 Acceleration from model (simulated)
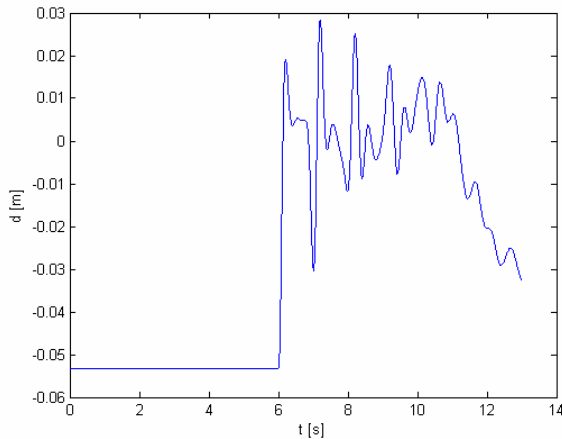
Figure 7-10 non-filtered calculated movement using acceleration data from simulated model
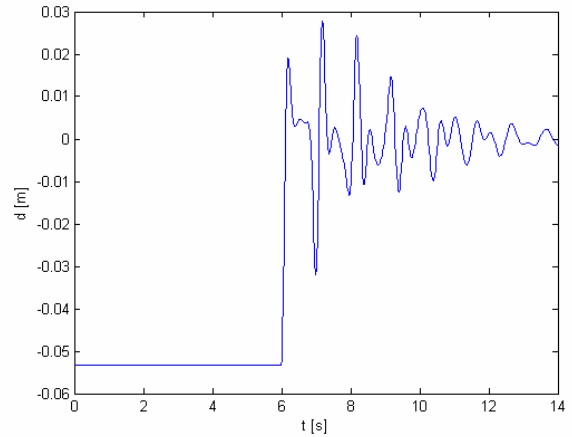
Figure 7-11 movement from model (simulated)

M-files eventually other input data are on enclosed CD in directory - Movement_CA_model.

7.4 Reasons of incorrectness of time integration

7.4.1 Numerical integration

Real generated acceleration is continuous curve and is represented in Figure 7-12 by red colour. But I cannot observe this curve, but I am able to observe discrete points with sampling frequency (in my case 200Hz) represented by blue dots. If I suppose zero noise of measurement, blue dots are on the red curve. I need to twice numerically integrate acceleration to observe position. First integration is shown below.

Correct integration:

$$\mathbf{v}(t) = \int_{37,5ms}^{t} \mathbf{a}(\tau) \cdot d\tau + v(37,5ms) \tag{7.1}$$

Numerical integration:

$$v(40ms) = a(40ms) \cdot dt + v(35ms) = 10 \cdot 5 + v(35ms) \tag{7.2}$$

Difference between these ways of integration is represented by green colour in figure below. If there was no difference between those two integrations, areas "A" and "B" would be the same. But they are not the same and difference between integrations is represented by difference between areas "A" and "B". And integrating a second time to get the position will lead to further error in calculation, given the already distorted value observed by first integration.
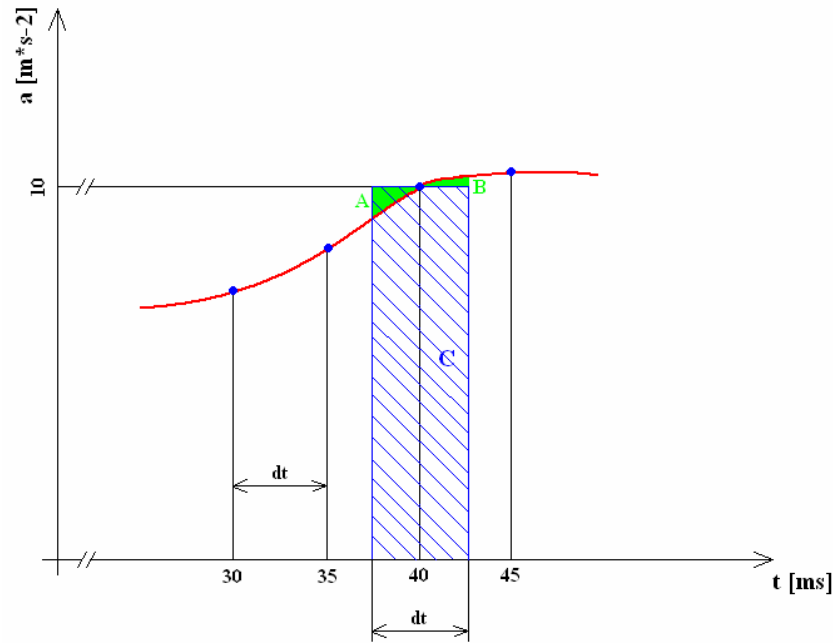
Figure 7-12 Numerical integration of discrete points

7.4.2 Noise of measurement

In the caption above I have supposed zero noise of measurement. But in the real world there is no way to know exact values. In each step I observe exact value plus noise and I do not know how big the noise is and how big exact value is. I just work with observed values. My observation (blue dots) in comparison with real values is shown in Figure 7-13.
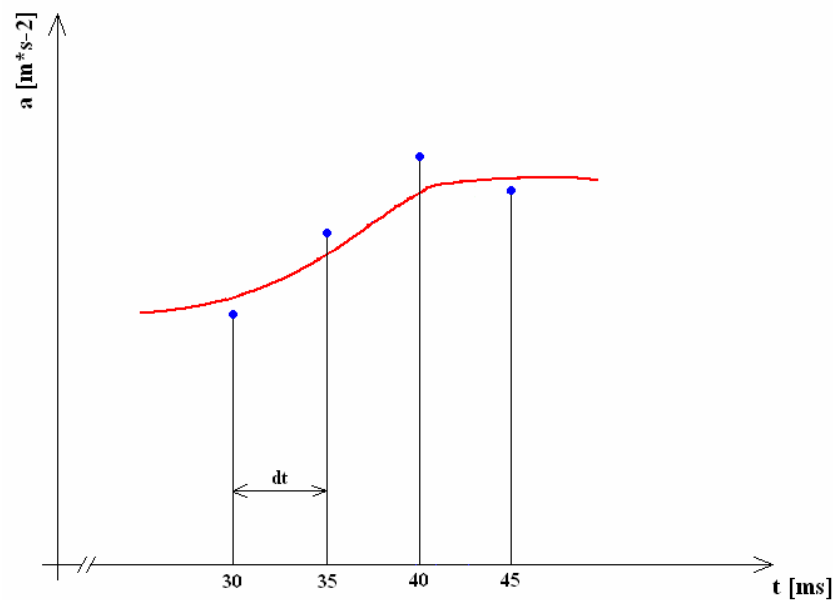

Figure 7-13 Measurement error

7.4.3 Error Propagation

As you can see at the beginning of chapter 4, Measuring Devices, each calculation step considers values from previous step such that error from previous step is growing with each step.

As one second calculation is done in 200 time steps, the above mentioned errors will grow with error propagation resulting in a simulation totally unusable within a few seconds.

For example if I would have error in acceleration about $er1 = 0.1 m \cdot s^{-2}$:

$$er2 = \frac{1}{2} \cdot er1 \cdot t^2 = 0.5 \cdot 0.1 \cdot 10^2 = 5m \qquad (7.3)$$

It causes error 5m in position in ten seconds!

The problem continuing even with using Kalman filtering.

7.5 Summary of vertical movement reconstruction

It is possible to reproduce movement only in a few seconds from the reasons as mentioned above in case of known initial conditions. Even if the Ampacimon device is in steady state, there is no zero acceleration and I observe some noise shown in Figure 7-14 and it causes that in simulation is not device in the same position before releasing as is shown in Figure 7-15. Again is observed acceleration and non-filtered observed position represented by blue colour and filtered values are represented by red colour.
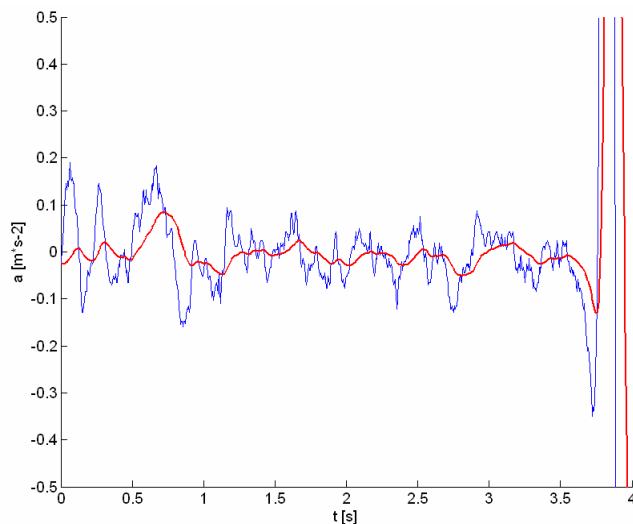
Figure 7-14 Acceleration in steady state   *Figure 7-15 Movement in steady state*
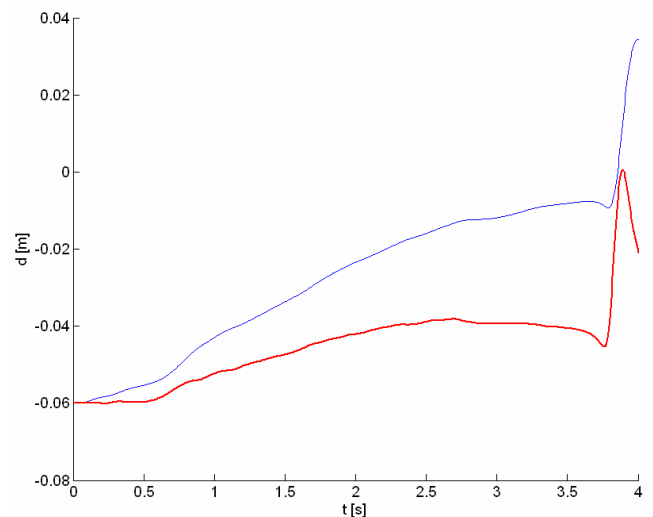
Another reason why that are those two movements different is that I do not know all details about the Canadian experiment and even observed values from measurement and model should be done in different conditions.

Last reason what I will mention is that even if I will know all of the details of experiment, in real world it will be a little bit different than in simulation by method of finite elements. Comparison is in Figure 7-16 and in Figure 7-17.
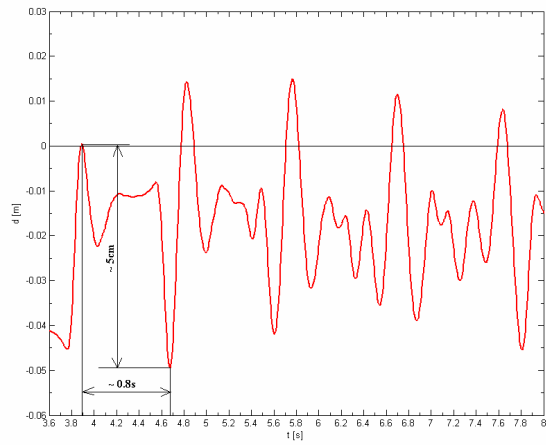
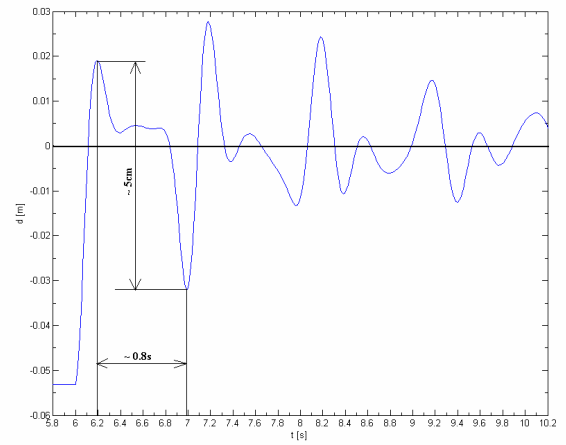*Figure 7-16 Observed movement from meas.*

Figure 7-17 Movement observed from model

8 2D MOVEMENT RECONSTRUCTION EXPERIMENT

For these experiments were used special built device with two 2D accelerometers and two linear gyroscopes. Data sheets are attached on enclosed CD. Device is supplied by 9V battery and connected by RS232 to PC. Data are collected by program Netbeans.
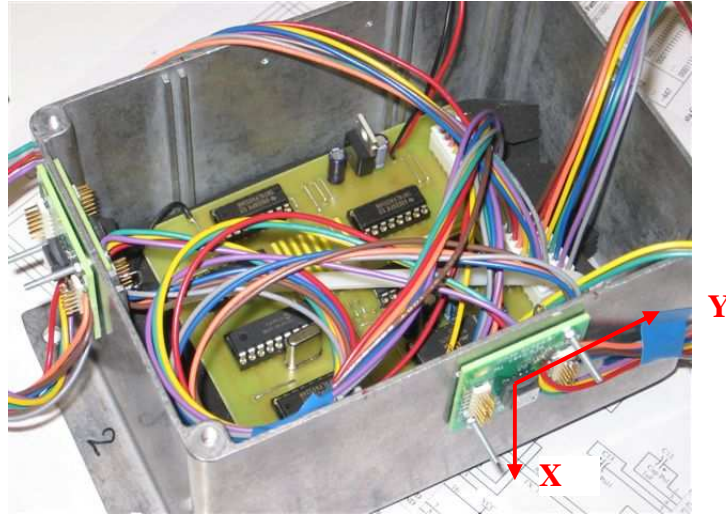

Figure 8-1 Measuring device

First of all is necessary to calibrate the accelerometers in all axes. Is necessary to measure +G and –G and then set offset and conversion factor. I did these experiments only with one 2D accelerometer.

Table 8-1 Calibrating table

axis and direction	measured	count	offset	count/G
- X	1223,7	-824,3	+9,45	814,85
+X	2853,4	805,4		
- Y	1223,5	-824,5	+3,3	821,2
+Y	2865,9	817,9		

Example:

$$count_{-X} = measured_{-X} - 2048 = 1223,7 - 2048 = -824,3 \tag{8.1}$$

$$offset_X = \left(count_{-X} + count_{+X}\right)/2 = \left(-824,3 + 805,4\right)/2 = 9,45 \tag{8.2}$$

$$count/G_X = \left(count_{+X} - count_{-X}\right)/2 = \left(805,4 + 824,3\right)/2 = 814,85 \tag{8.3}$$

8.1 Without rotation

The first experiment was making a simple movement of the measuring device from left to right, then up and down in one row, about tens of centimetres in each direction.
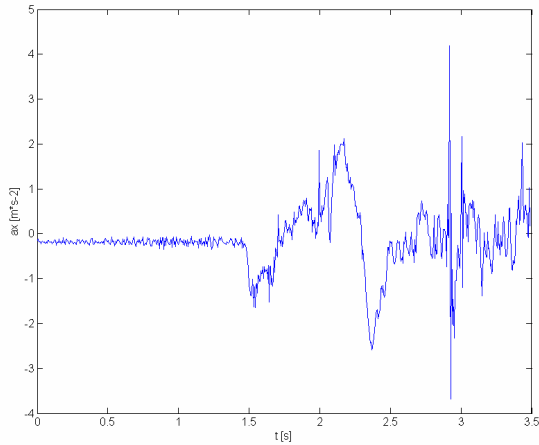
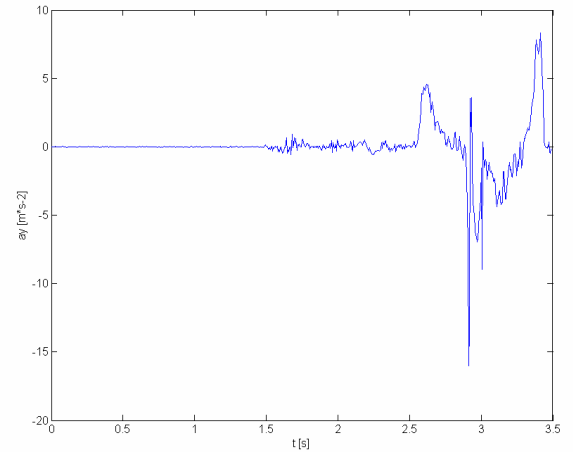*Figure 8-2 Measured acceleration in x axis*

Figure 8-3 Measured acceleration in y axis

As you can see from Figure 8-2 even in steady state in first 1,4s is not the acceleration (or average of noisy acceleration) equal to zero and first 1,4s will be used for additional offset setting. It is caused by angle between "x" axis and acceleration due to gravity which is not exact 90° and a small part of mentioned acceleration is even in "x" (horizontal) direction.
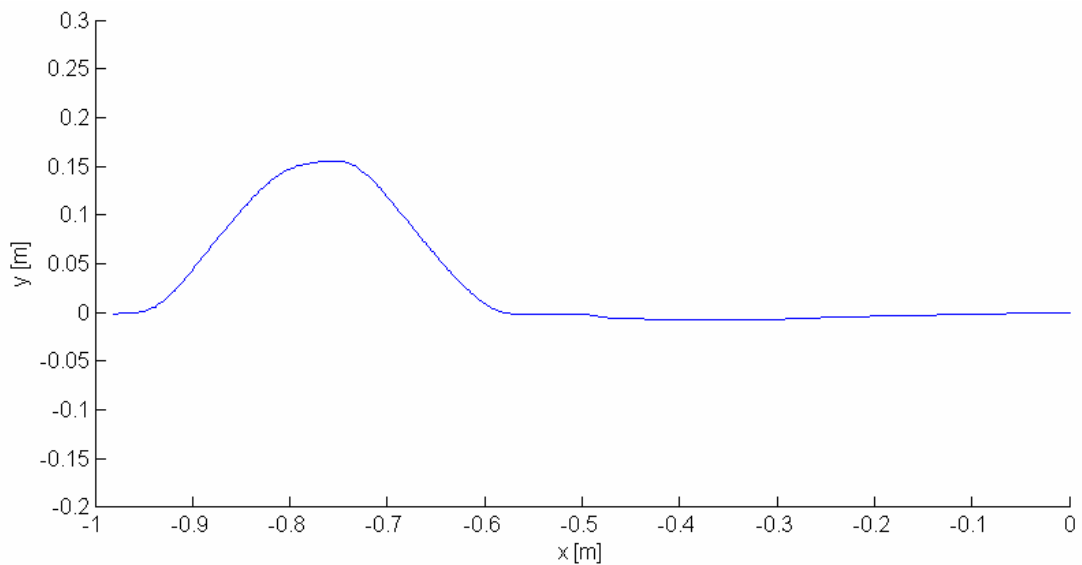

Figure 8-4 Reconstruction from measurement (drift is due to the offset in x axis)
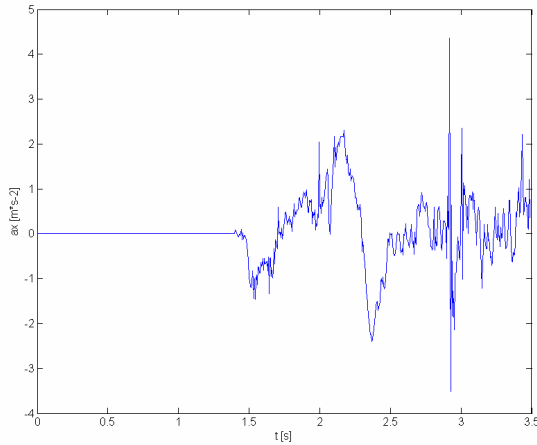
Figure 8-5 Observed acceleration in x axis with 1.4s calibration
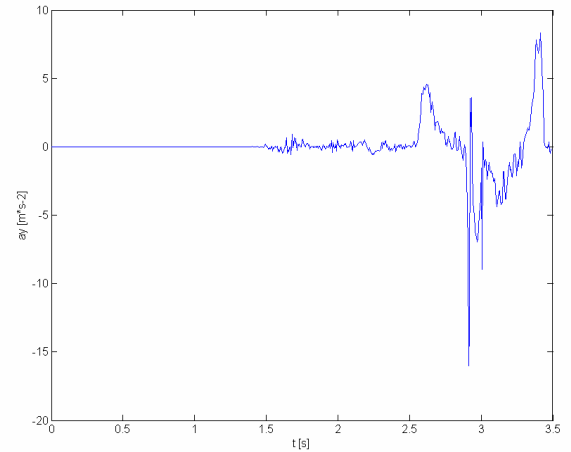
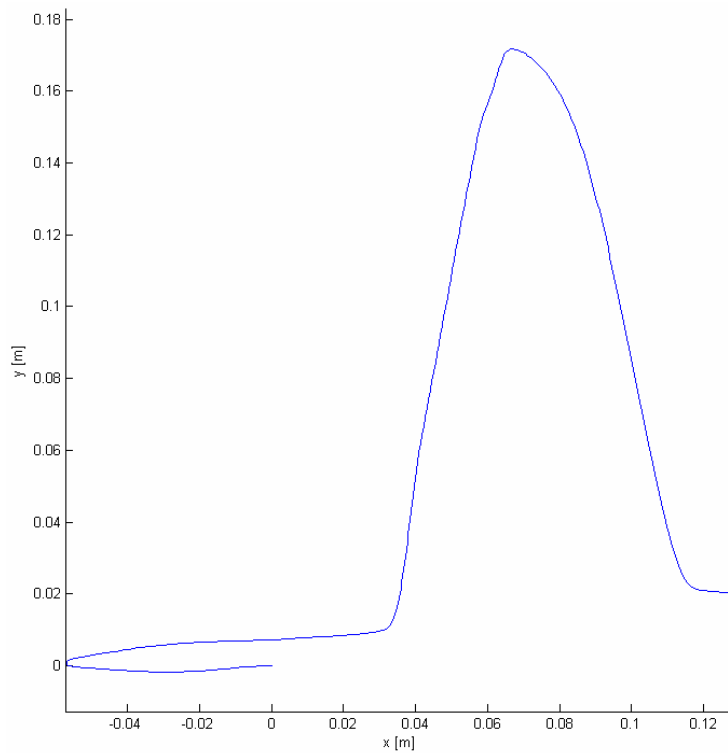*Figure 8-6 Observed acceleration in y axis with 1.4s calibration*

Figure 8-7 Observed movement after calibration

As you can see from Figure 8-7 here is final movement closer to real movement, but subtraction of negative acceleration was exceeded a little bit. By experimental modification of the signal should be finally found movement very similar to real movement, represented in Figure 8-8.
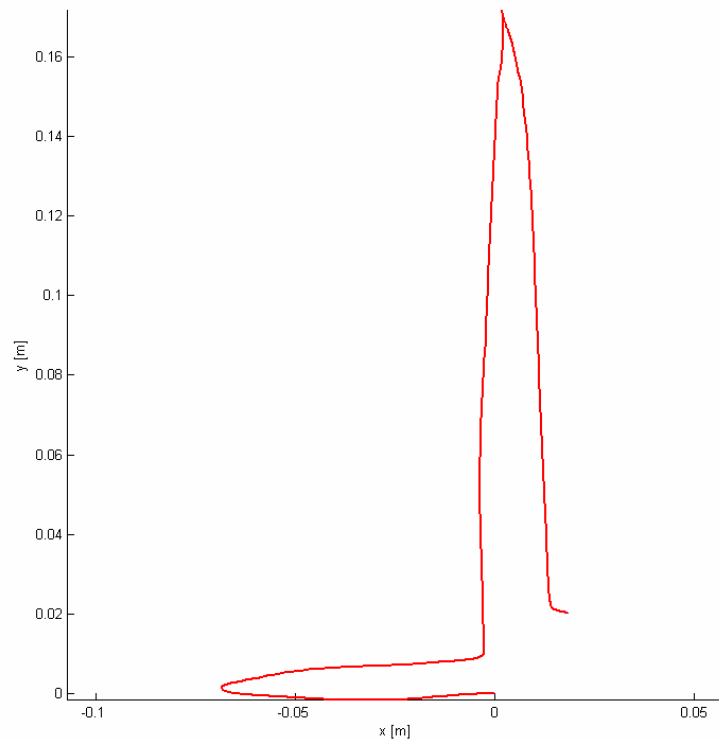
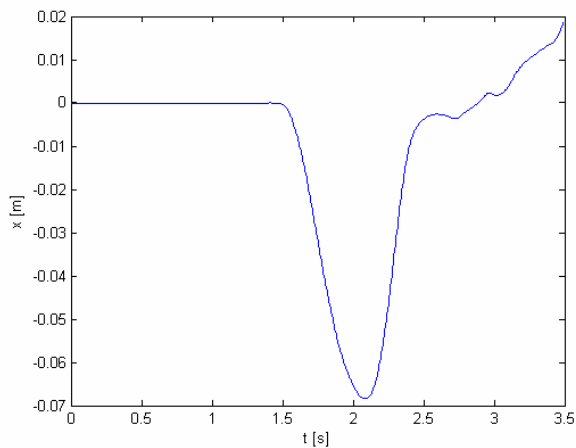*Figure 8-8 Observed movement after calibration and experimental modification*
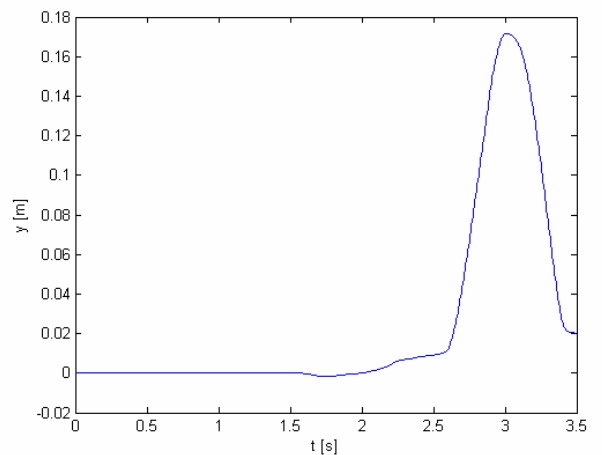

Figure 8-9 Observed x position in time

Figure 8-10 Observed y position in time

8.1.1 Conclusion

In the caption above a very easy experiment was done with 2D accelerometer. After calibrating the device, there was still a small part of acceleration due to gravity applied in x axis. This part was integrated for the first 1.4s and average of this value was applied on accelerations in x axis to be corrected. The result of observed position is in Figure 8-7. As you can see there is a small part of positive acceleration in x axis to be removed experimentally. After that correction was observed final Figure 8-8. Real movement was similar to that, but error is very serious if I will take into consideration time of integration only 2.1s and no rotation were take into consideration. Of course it is impossible to make movement with device with no rotation, so I cannot say now, it is possible to continue by this way, or if it is totally useless.

8.2 With rotation

Now I will take into consideration even information from gyroscope. In Figure 8-12 is observed angle between moving and global axes. As mentioned above, this movement was just vertical and horizontal movement without rotation, but it is impossible to do it with no rotation, so small angular velocities were observed as you can see in Figure 8-11.
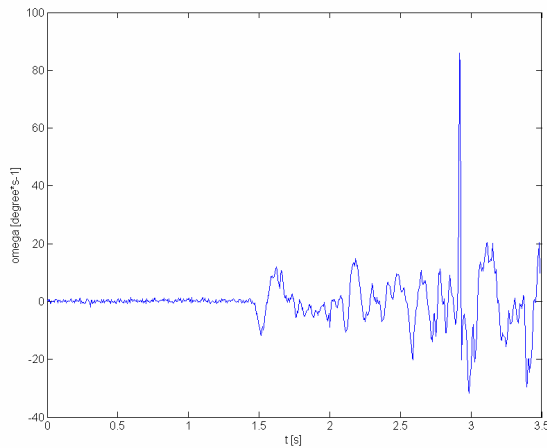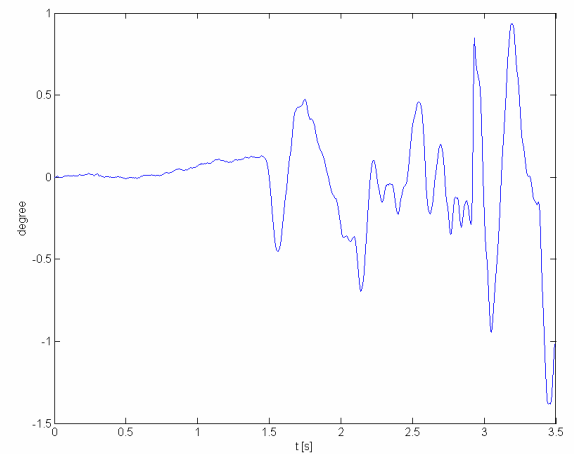

Figure 8-11 Observed angular velocity

Figure 8-12 Observed angle of rotation

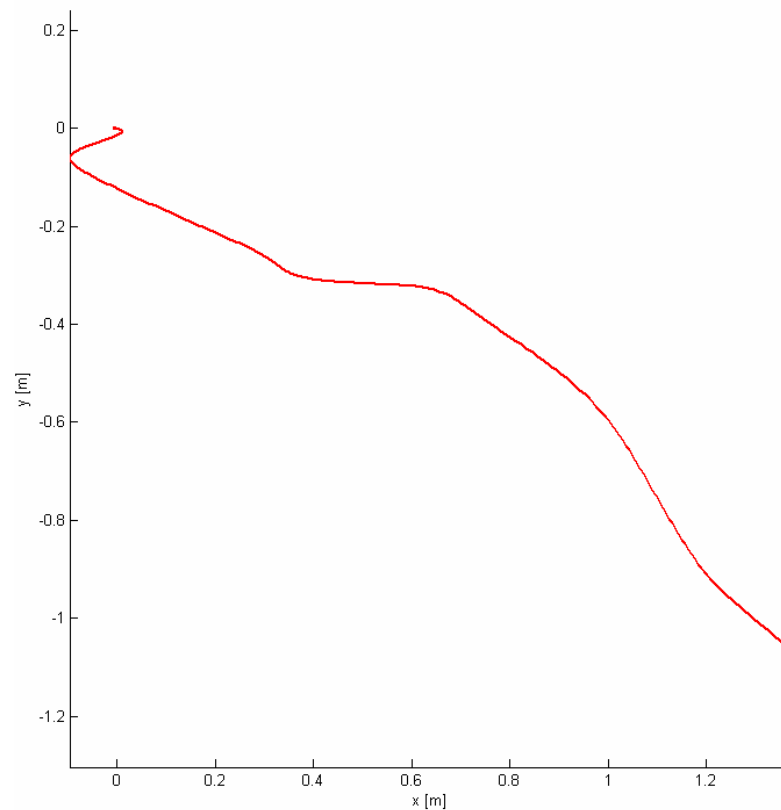Let's have a look on results, if they will be better or worse.

Figure 8-13 2D movement with gyroscope

As you can see in Figure 8-13 the movement is totally different from original one and it is impossible to reproduce movement based only on measurement of accelerometers and gyroscope.

On earth there is a permanent acceleration of 1g, if the orientation horizontally is off by the biggest error represented in Figure 8-12, say, one degree, we will get an acceleration error e_1:

$$e_1 = \mathbf{g} \cdot \sin 1° = 0,1712 m \cdot s^{-2} \tag{8.4}$$

Integrating the acceleration error e_1 twice, this results in an accumulated position error e_2 after 10 seconds of:

$$e_2 = 0,5 \cdot e_1 \cdot t^2 = 0,5 \cdot 0,1712 \cdot 10^2 = 8,56 m \tag{8.5}$$

M-files eventually other input data are on enclosed CD in directory - Movement_2D.

8.2.1 Conclusion

In the caption above, an experiment of movement reconstruction in a plane was performed. In plane, there are three degrees of freedom, two translations and one rotation; two devices were used for measurement, one 2D accelerometer and one gyroscope. With that device was done very easy movement for reconstruction. Result of this experiment is in Figure 8-13 and is totally different from the original one. This type of movement reconstruction is called "open loop" and for our usage is unusable even for first few seconds. Error propagation is illustrated in Figure 8-14 and Figure 8-15.
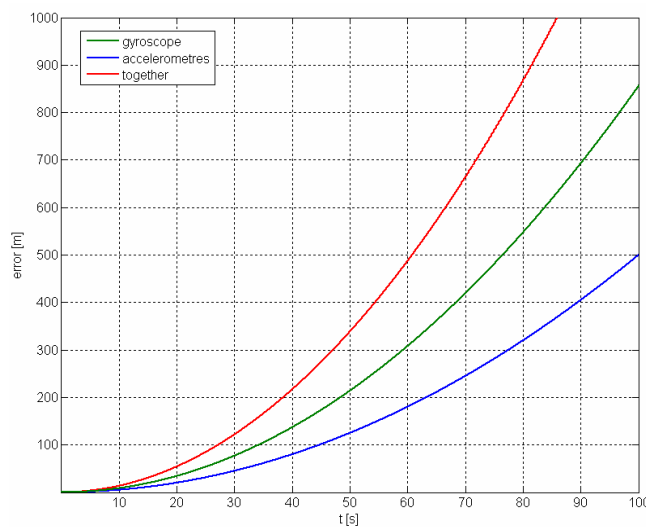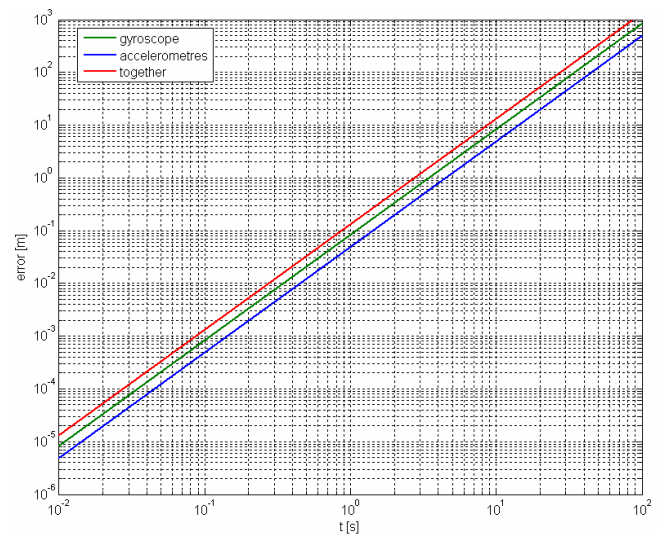

Figure 8-14 Error propagation

Figure 8-15 Log-Log error propagation

Solution should be found in usage of Kalman filter to combine or fuse information from different sensors. The basic idea is to use the Kalman filter to weigh the different mediums most heavily in the circumstances where they each perform best, thus providing more accurate and stable estimates than a system based on any one medium alone. The indirect feedback Kalman filter shown in Figure 8-16 (also called a complementary or error-state Kalman filter) is often used to combine the two mediums. In such a configuration, the Kalman filter is used to estimate the difference between the current inertial and optical (or acoustic, magnetic, GPS or combination of them) outputs, it continually estimates the error in the inertial estimates by using the optical (e.g.) system as a second reference. This error estimate is then used to correct the inertial estimates. In our application is correction of position by GPS unusable because of low precision of about one meter but GPS get very precise information about velocity and velocity could be corrected by GPS.
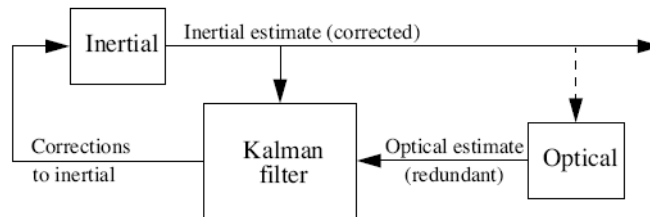
Figure 8-16 The Kalman filter used in an indirect-feedback configuration to optimally weight inertial and optical information. [7]

9 DETERMINING LINE POSITION USING G-DIRECTION

9.1 Using real data from Ampacimon

Ampacimon device is placed on line near the coast in Belgium and is measuring continuously with sampling frequency 12,5Hz and sending data by GSM network to Montefiore Institute.
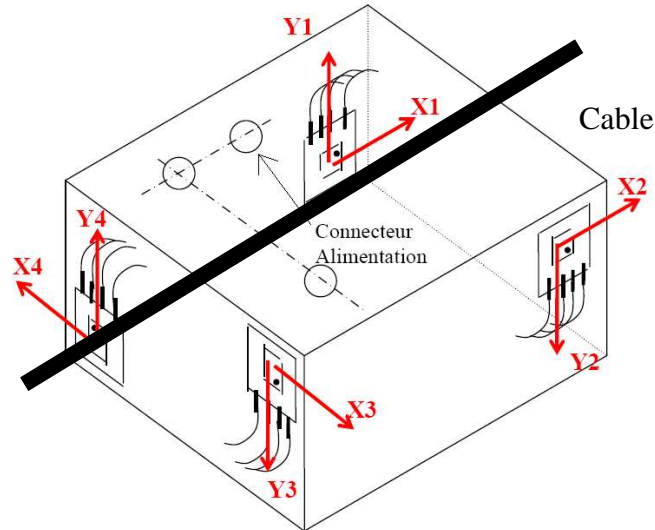

Figure 9-1 Accelerometers position and orientation in Ampacimon

I am interested in axes „X3" and „Y3" of module „1" and using data measured 12.1.2009 and try to determine position of the cable using steady orientation of acceleration due to gravity. Explained in Figure 9-3.

Figure 9-2 Offsets and conversion factors

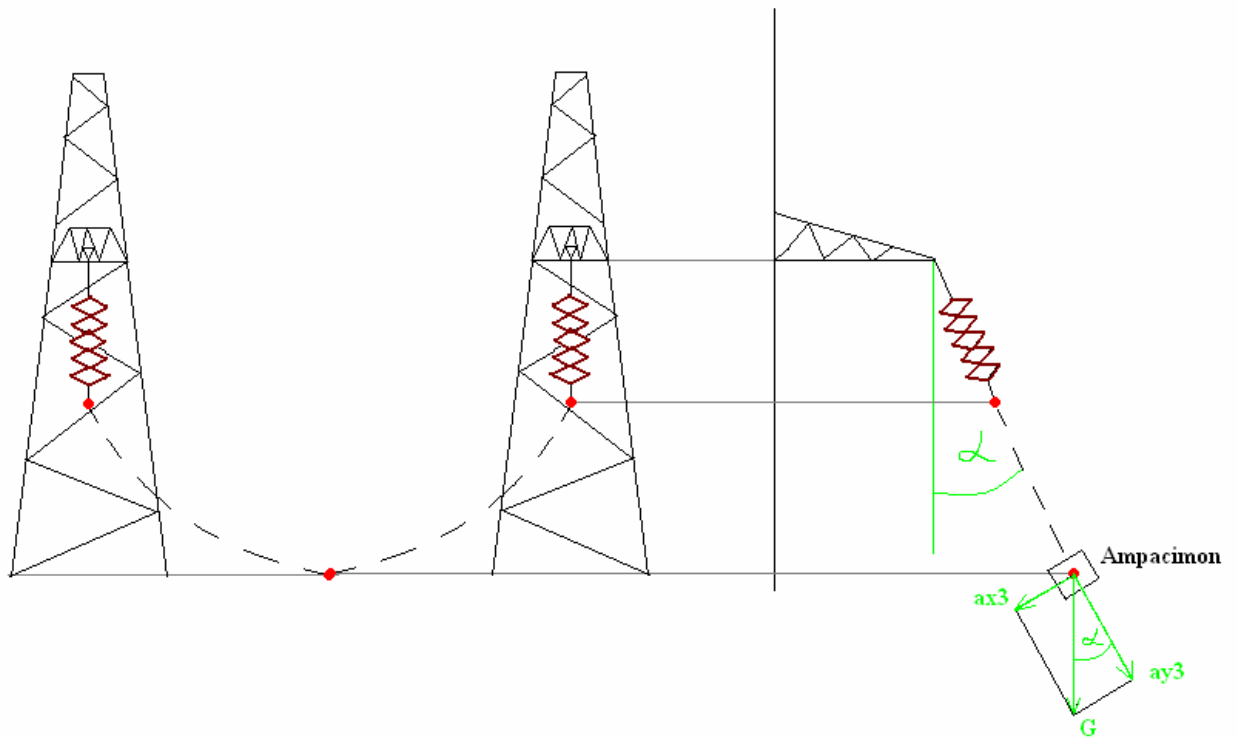| axis name	axis number	Module	Accelerometer reference	Offset [count]	Conversion factor [count/G]
Y1	1	1	1E001	16.5	770
X3	4	1	1E002	-9.5	774.5
Y3	5	1	1E002	-16.5	770.5
Y1	1	2	1E007	-7	778
X3	4	2	1E008	-35.5	773.5
Y3	5	2	1E008	10	770
Y1	1	3	1E011	-3.5	773.5
X3	4	3	1E012	-13	769
Y3	5	3	1E012	-17	770
Y1	1	4	1E013	-17	775
X3	4	4	1E014	-2	773
Y3	5	4	1E014	-15.5	770.5

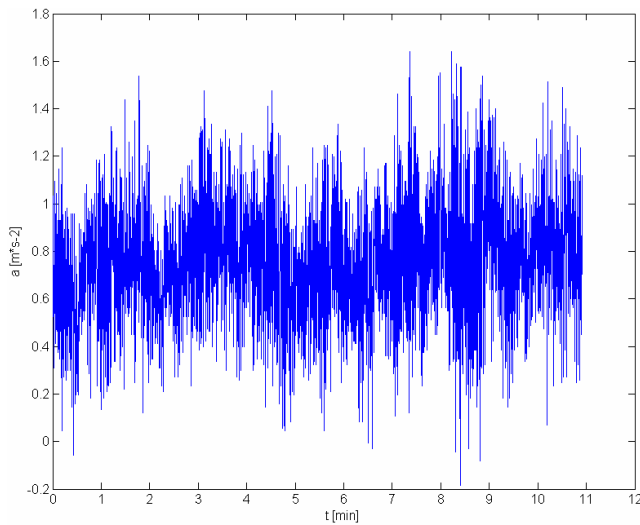*Figure 9-3 Position of line between span in wind condition*

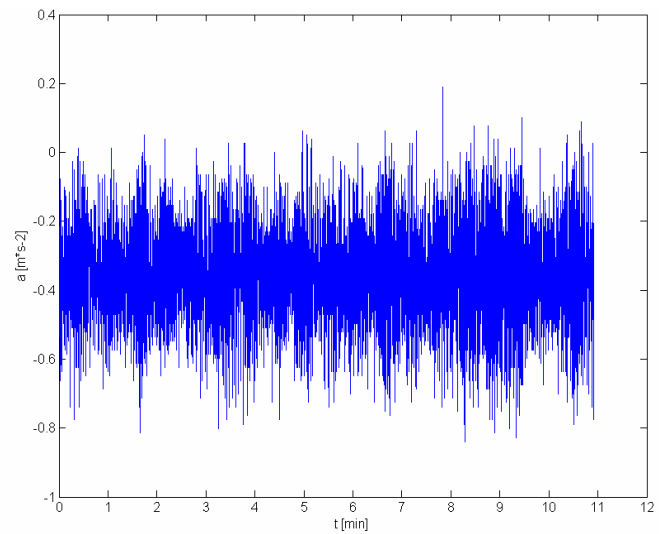*Figure 9-4 Horizontal acceleration*

Figure 9-5 Vertical acceleration

Because measurement is very noisy and I am interested only in low-frequency large movement, I will do FFT and I will use only low frequency component and DC component.
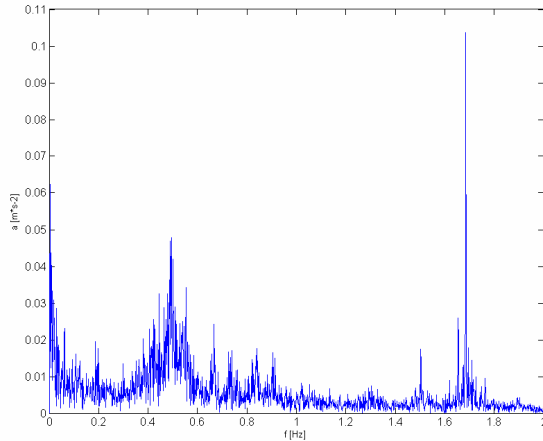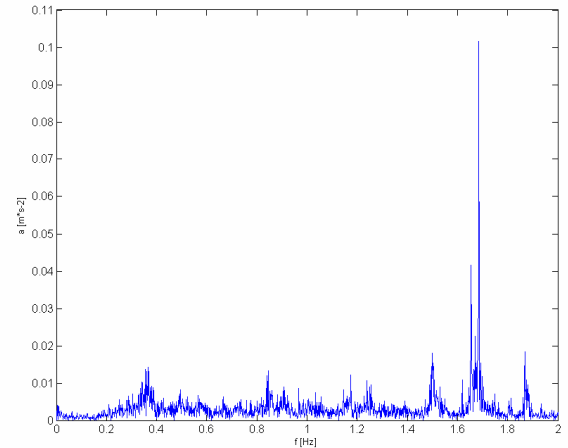
Figure 9-6 FFT of horizontal acceleration

Figure 9-7 FFT of vertical acceleration

In Figure 9-6 is FFT of horizontal acceleration without $0,7539 m \cdot s^{-2}$ DC component and in Figure 9-7 is FFT of vertical acceleration without $9,4512 m \cdot s^{-2}$ DC component. When I have a look on low frequencies (e.g. <0,5Hz) there aren't expressive components corresponding huge movement. I don't have real measurement of really huge movement and I will use model of line to observe accelerations corresponding huge movement in the next chapter. From the FFT is seen expressive component of about 1,7Hz and is possible to say that it is probably Aeolian vibration. Average angle of line deflexion could be observed due to constant orientation of acceleration due to gravity.

Average angle α:

$$\alpha = \arctan\left(\frac{ax3_{DC}}{ay3_{DC}}\right) = \arctan\left(\frac{0,7539}{9,4512}\right) = 4,56° \qquad (9.1)$$

It will be discussed more deeply in the next chapter.

M-files eventually other input data are on enclosed CD in directory - Ampacimon_real_data.

9.2 Using data observed from model of span

Because I don't have measurement from huge movement, I will use model of span to simulate huge movement and I will work with observed accelerations. Observed acceleration from a simulation program (SAMCEF Field V6.3) is in absolute axes and without acceleration due to gravity (9,81 m*s^{-2}). From information about displacement is counted angle of line deflection, acceleration due to gravity is added to the vertical axis and information about acceleration is recounted to relative axes respectively. Then is applied Gaussian noise with signal to noise ration (SNR) 10dB. Now I have input data for processing.

Details of model:

- Left pylon is 58m high, right one is 55 m and distance between them is 448,23 m. Line is fixed on pylons.

- Two forces are simulated wind

- Initial condition – stress in the middle of span is 24 514 N

- Average length of element is 2,5 m

Table 9-1 Parameters of span model

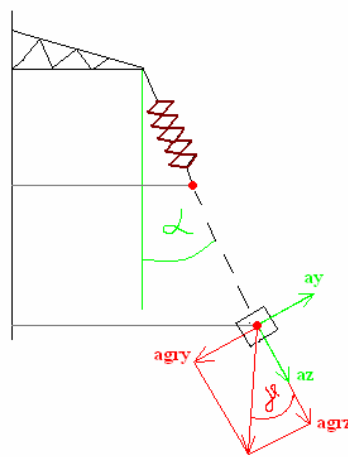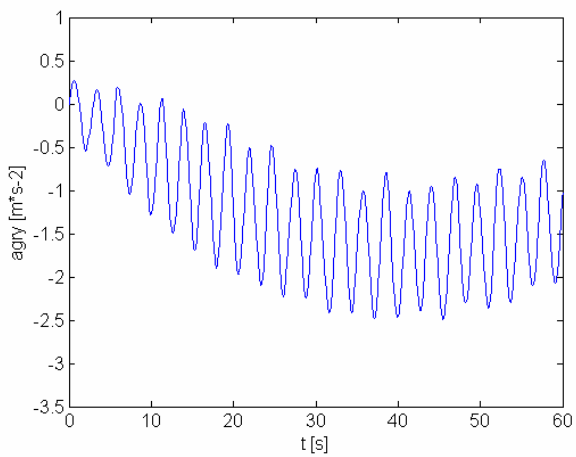| Mass per unit length	1,713	kg/m
Rated strength	20	kN
Diameter	31,5	mm
Area	621	mm^2
Module of elasticity	59	GPa
Dilatation coefficient	23	$10^{-6}/°C$

Figure 9-8 Orientation of axes

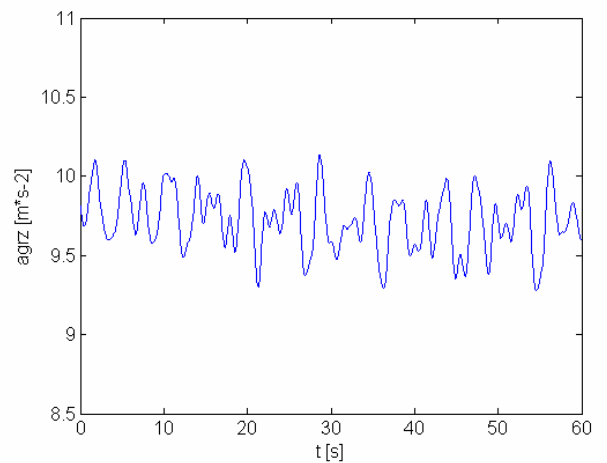*Figure 9-9 Exact horizontal acceleration*

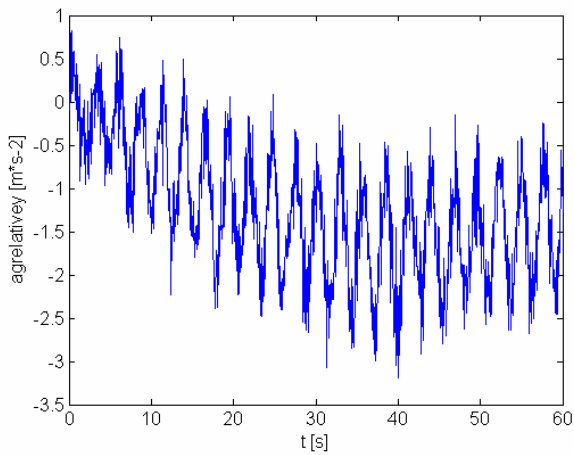*Figure 9-10 Exact vertical acceleration*
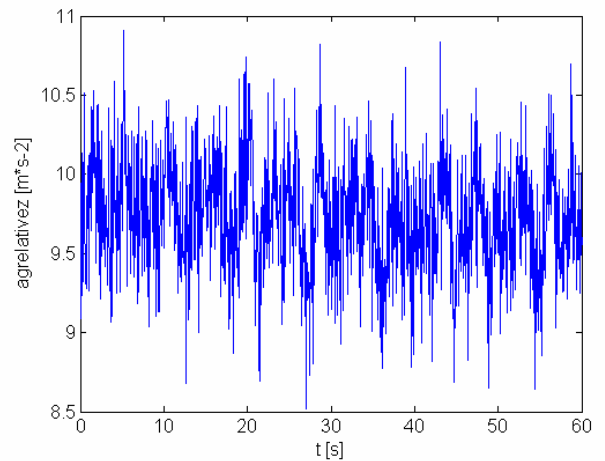
Figure 9-11 Noisy horizontal acceleration

Figure 9-12 Noisy vertical acceleration

Because measurement is very noisy and I am interested only in low-frequency huge movement, I will do FFT and I will use only low frequency components and DC component.
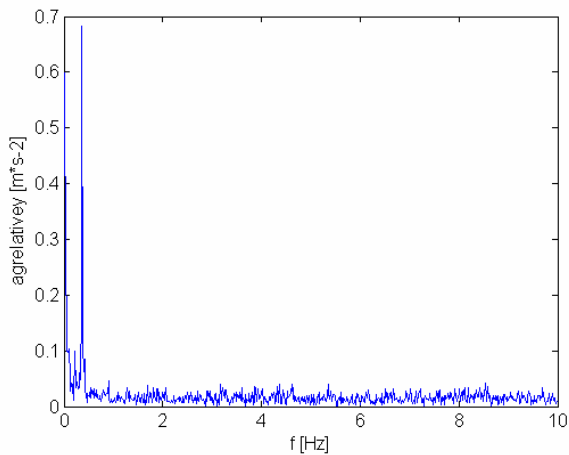

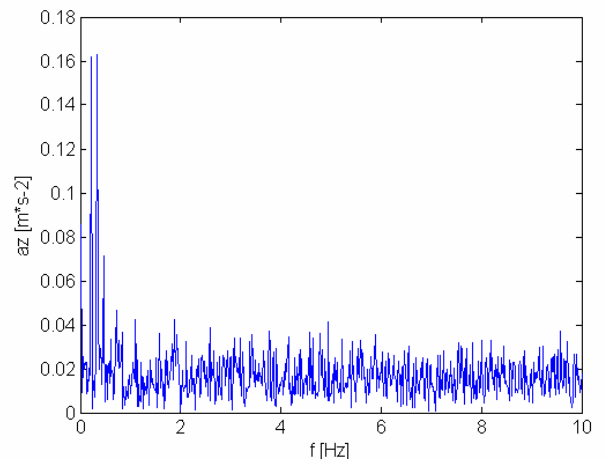*Figure 9-13 FFT of horizontal acceleration*

Figure 9-14 FFT of vertical acceleration

In Figure 9-13 is FFT of horizontal acceleration without $-1,2003 m \cdot s^{-2}$ DC component and in Figure 9-14 is FFT of vertical acceleration without $9,7264 m \cdot s^{-2}$ DC component. Frequency resolution is 601 values. (Sampling frequency is 20Hz.)

To subtract noise eventually other type of motion I will tag together signal from FFT using low frequencies and high amplitudes only. For example if I want to take only dominant parts of FFT I will take into consideration frequencies below 0,5Hz and amplitudes over 0,1 in horizontal acceleration and 0.05 in vertical acceleration. For usage in the real world it should be defined by relative values, but in this one case I am using absolute values. Algorithm for signal reconstruction and all other signal processing is in m-file on enclosed CD.
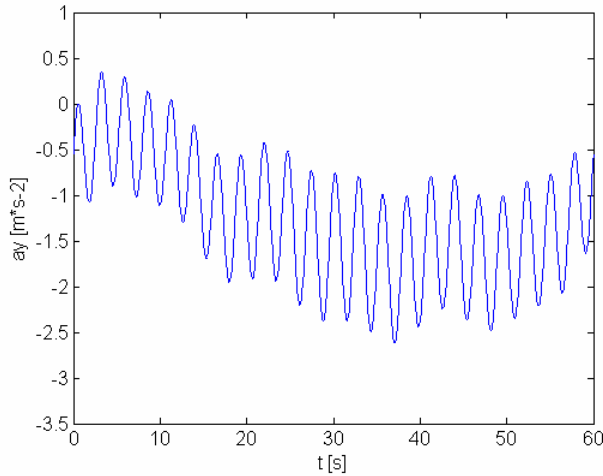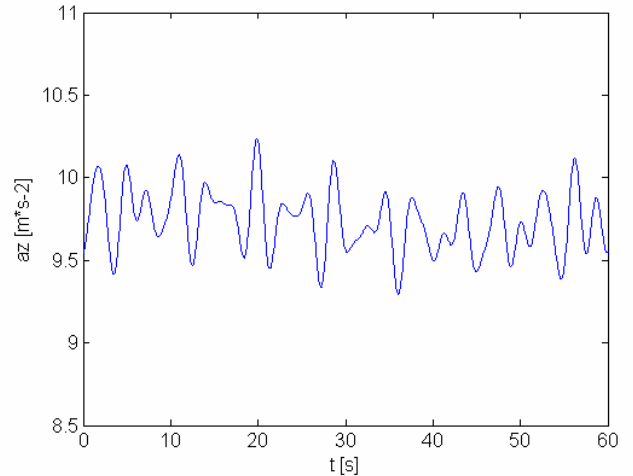
Figure 9-15 Reconstructed horizontal acceleration

Figure 9-16 Reconstructed vertical acceleration

Angle γ:

$$\gamma = \arctan\left(\frac{\mathbf{ax}}{\mathbf{ay}}\right) \tag{9.2}$$

Than should be compared angle of deflexion with angle γ.
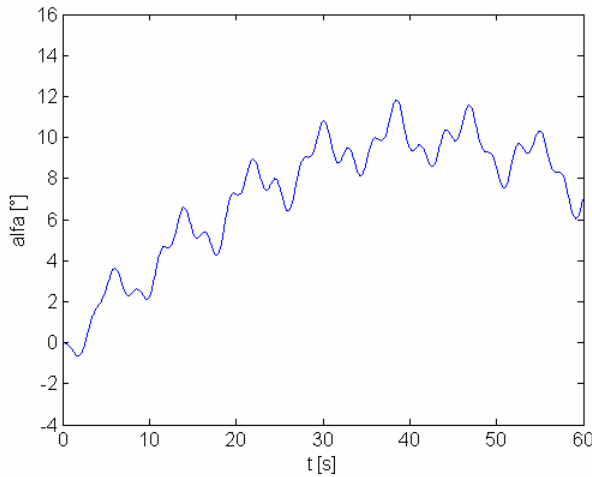
Figure 9-17 Exact angle of deflection
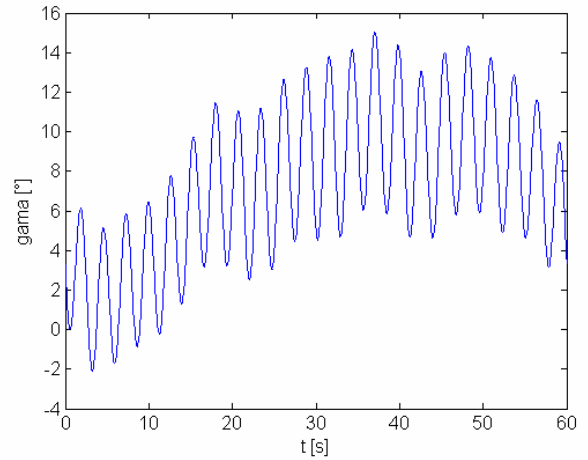
Figure 9-18 Angle γ

9.3 Conclusion

Result of angle γ depends on parts of FFT which are taken into consideration and should be different but it is difficult to say which result is the best. For example if I subtract dominant part around 0.5Hz in horizontal acceleration result of angle γ will be different and is in Figure 9-19. But the most important information is about maximum angle of deflection and it is known really precisely and it is a little bit less than 12°. Better results could be observed using Kalman filtering with combination of information from gyroscope.

Figure 9-19 Angle γ

    M-files eventually other input data are on enclosed CD in directory - Simulation_huge_ movement.

10 SUMMARY

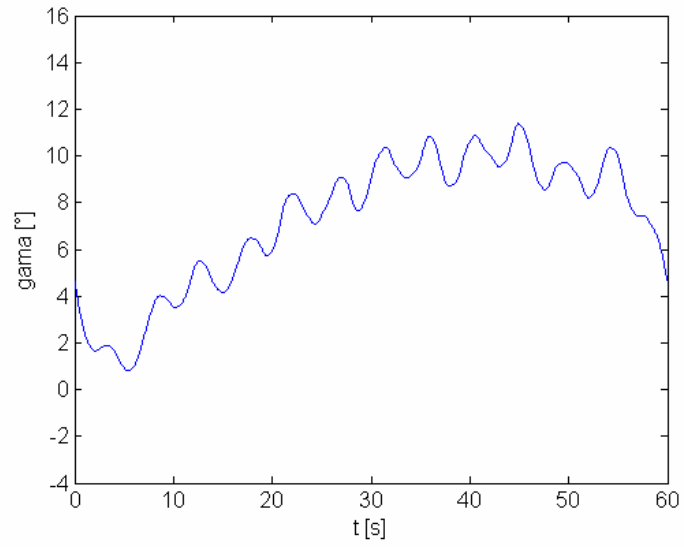The main aim of this thesis was to be able to reconstruct huge movements of overhead lines based on measurement from accelerometers and gyroscopes using Kalman filtering. I started only with acceleration in one axis and tried to rebuild the movement.
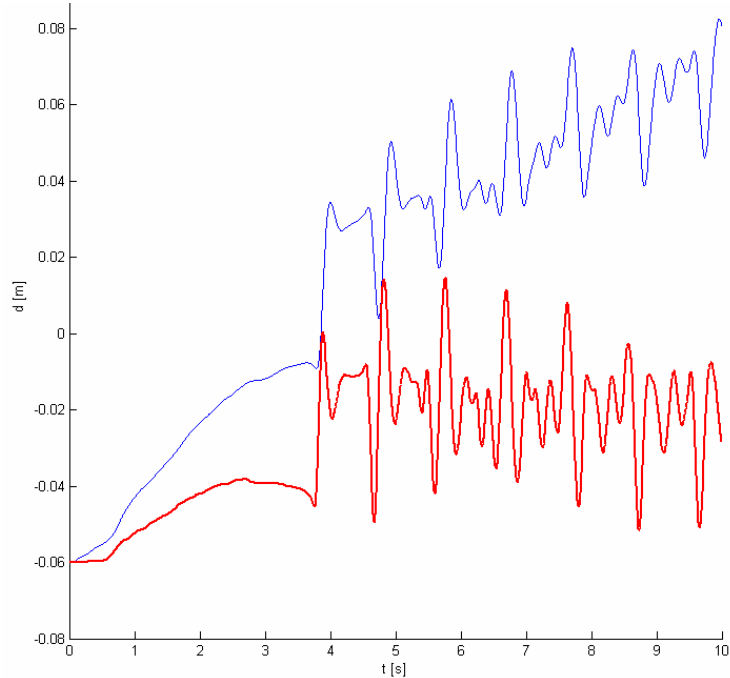
Figure 10-1 Non-filtered observed (blue) and filtered (red) position by Kalman filter

Due to the fact that I suppose initial velocity is zero, but it should be a little bit more than zero and due to the fact that each step are used values from previous step and actual values are never corrected by other external system is in Figure 10-1 shift of position. It is impossible to reconstruct signal only from known accelerations. Moreover I don't know all the details about this experiment and real result either so I decided to do my own experiment with measuring devices to be sure about initial conditions and related details.

I took the box with measurement devices and did simple movement about tens centimetres to left and back and then up and back.

Figure 10-2 Observed movement after calibration

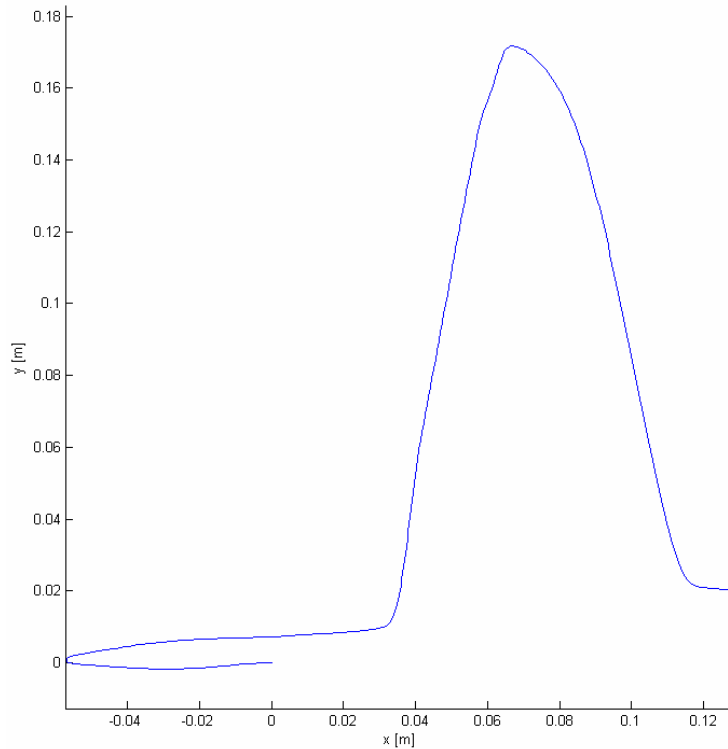As you can see the result is different than the movement I did. Moreover I didn't take into consideration measurement from gyroscope and I did movement without rotation. Using even measurement from gyroscope is reconstructed movement totally different than original one.

For this reconstruction algorithm called "open loop" was used, it means that I took velocity and position from previous step and never correct them by indirect-feedback for example. It causes big error due to error propagation in few seconds.
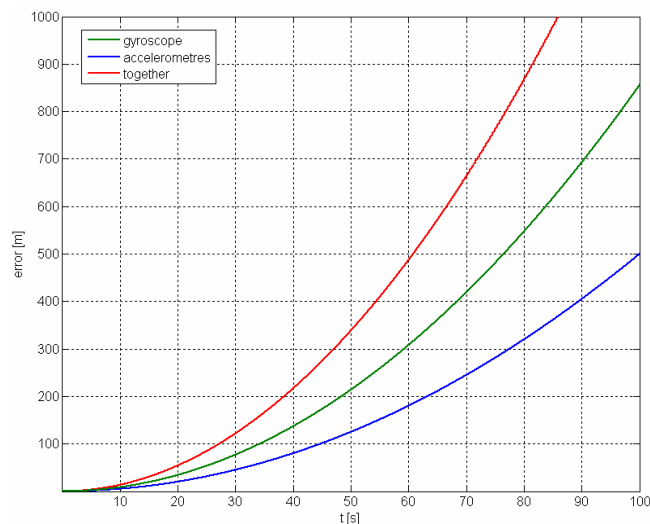
Figure 10-3 Error propagation

Solution should be found in usage of Kalman filter to combine or fuse information from different sensors. The basic idea is to use the Kalman filter to weigh the different mediums most heavily in the circumstances where they each perform best, thus providing more accurate and stable estimates than a system based on any one medium alone. The indirect feedback Kalman filter shown in Figure 10-4 (also called a complementary or error-state Kalman filter) is often

used to combine the two mediums. In such a configuration, the Kalman filter is used to estimate the difference between the current inertial and optical (or acoustic, magnetic, GPS or combination of them) outputs, it continually estimates the error in the inertial estimates by using the optical (e.g.) system as a second reference. This error estimate is then used to correct the inertial estimates. In our application is correction of position by GPS unusable because of low precision of about one meter but GPS get very precise information about velocity and velocity could be corrected by GPS.
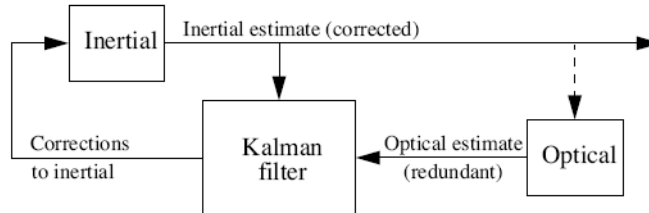

Figure 10-4 The Kalman filter used in an indirect-feedback configuration to optimally weight inertial and optical information. [7]

How to know exact initial position or how to correct position time to time remain unanswered questions to be solved in future.

Other approach to line position was done using the fact that acceleration due to gravity has the same direction all the time. To subtract noise and high frequencies was used FFT which took into consideration only dominant parts of FFT in low frequencies part. Then was counted angle between accelerations in two axes where acceleration due to gravity is applied. See Figure 9-17, Figure 9-18 and Figure 9-19 for results. More precise result should be observed subtracting acceleration causing movement and have only acceleration due to gravity divided in axes. It could be done using Kalman filter with indirect-feedback with information about angle of deflection from gyroscope.

REFERENCES

[1]   LILIEN, J., L., *Ampacimon presentation 2008,* University of Liege, 6 pages, 2008

[2]   PALO ALTO, *Transmission Line Reference Book: Wind-Induced Condactor Motion.* EPRI, CA, USA 618 pages, 1012317, 2006

[3]   KIESSLING, F., NEFZGER, P., NOLASCO, J.F., KAINTZYK, U. *Overhead Power Lines,* Berlin, Germany, Springer, 759 pages, ISBN: 978-3-540-00297-0, 2003

[4]   SIMON HAYKIN, *Kalman filtering and neural networks,* McMaster University, Hamilton, Ontario, Canada, A Wiley-Interscience Publication, 284 pages, ISBN 0-471-36998-5, 2001

[5]   *Kalman filter,* http://en.wikipedia.org/wiki/Kalman_filter

[6]   FAJMON, B., RŮŽIČKOVÁ I., *Matematika 3*, BUT, 254 pages

[7]   WELCH, G., BISHOP, G., *An Introduction to the Kalman Filter*, University of North Carolina, Chapel Hill, NC, USA, 81 pages

[8]   MATLAB HELP - http://www.mathworks.com/access/helpdesk/help/techdoc/

[9]   LUINGE, H., J., VELTING, P., H., *Measuring orientation of human body segments using miniature gyroscopes and accelerometers,* University of Twente, Enschede, Netherlands, pages 273-282, 2005

[10] WILLIAMSON, R., ANDREWS, B., J., *Detecting absolute human knee angle and angular velocity using accelerometers and rate gyroscopes*, University of Reading, UK, pages 294-302, 2001

[11] GYROSCOPES - http://www.gyroscopes.org

[12] OMEGA.COM - http://www.omega.com

[13] LEBON, G., *Introduction a la mecanique rationnelle,* Universite de Liege, 304 pages

[14] MURPHY, K., *KALMAN FILTER TOOLBOX*, http://www.cs.ubc.ca/~murphyk/ /Software/Kalman/kalman.html, 1998

[15] http://blinkdagger.com/matlab/matlab-gui-tutorial-slider

[16] MAYBECK, S., P., *Stochastic models, estimation, and control,* Air Force Institute of Technology, Wright-Patterson Air Force Base, Ohio, Academic Press, New York, 16 pages, ISBN 0-12-480701-1 (v. 1)

[17] KORKA, A., D., *Kalman Filtering for an Aided Inertial Navigation System,* Massachusetts Institute of Technology, 70 pages, 1999

[18] LUTHI, P., MOSER, T., *Low Cost Inertial Navigation System,* Swiss Federal Institute of Technology Zurich, 47 pages, 2000

[19] GADE, K., *Introduction to Inertial Navigation and Kalman Filtering,* Norwegian Space Centre, 61 pages, 2008

[20] WOODMAN, J., O. *An introduction to inertial navigation,* Computer Laboratory, University of Cambridge, 37 pages, 2007

[21] *The MIDG II INS/GPS*, http://www.microboticsinc.com/ins_gps.html

[22] *Inertial Navigation System*, http://en.wikipedia.org/wiki/Inertial_navigation_system

[23] KING, A., D., *Inertial Navigation – Forty Years of Evolution,* Marconi Electronic Systems Ltd., 10 pages, 1998

[24] VIKAS, K., V., *Integration of Inertial Navigation System and Global Positioning System Using Kalman Filtering,* Indian Institute of Technology, Bombay, 69 pages, 2004

[25] WALCHKO, J., K., NECHYBA, C., M., SCHWARTZ, E., ARROYO, A., *Embedded Low Cost Inertial Navigation System,* University of Florida, Gainesville, 8 pages, 2003

[26] *A Strap Down System,* http://xenia.media.mit.edu/~verp/projects/smartpen/node8.html

[27] MADJAROV, A., *An Algorithm for Strapdown Inertial Navigation System*

[28] http://mafija.fmf.uni-lj.si/seminar/files/2007_2008/MEMS_accelerometers-koncna.pdf

[29] http://en.wikipedia.org/wiki/Microelectromechanical_systems